https://doi.org/10.5194/egusphere-2025-495
Preprint. Discussion started: 18 February 2025

A comparison of the last two glacial inceptions (MIS 7/5) via fully coupled transient ice and climate modeling

Marilena S. Geng[1], Lev Tarasov[1], and April S. Dalton[1]

[1]Department of Physical Oceanography, Memorial University of Newfoundland and Labrador, St. John's, NL, Canada

Correspondence: Marilena S. Geng (msgeng@mun.ca)

Abstract. Little is known about the evolution of continental ice sheets through the last two glacial inceptions (Marine isotope stages, MIS 7d and MIS 5d). Here, we present the results of a perturbed parameter ensemble of transient simulations of the last two glacial inceptions and subsequent interstadials (MIS 7e-7c, 240-215 ka and MIS 5e-5c, 122-98 ka) with the fully coupled ice/climate model LCice. LCice includes all critical direct feedbacks between climate and ice. As shown herein, it can capture the inferred sea level change (of up to 80 m) of the last two glacial inceptions within proxy uncertainty. One key underlying question of paleoclimate dynamics is the non-linear state dependence of the climate system. Concretely, in a model-centric context, to what extent does the capture of one climate interval in an Earth systems model guarantee capture of another interval? For LCice, the capture of present-day climate is insufficient to predict capture of glacial inception climate, as only a small fraction of ensemble members that performed "well" for present-day captured inception. Furthermore, the capture of inferred sea level change in one inception has weak correlation with the same outcome for the other.

After partial history matching against present-day and past sea level constraints, the resultant NROY (not ruled out yet) ensemble of simulations have a number of features of potential interest to various paleo communities, including the following. (i) In correspondence with the inferred last glacial maximum configuration, the simulated North American ice sheets are substantially larger than the Eurasian ice sheet throughout MIS 5d-MIS 5c and MIS 7d-MIS 7c. (ii) Hudson Bay can transition from an ice-free state to full ice cover (grounded ice) within 2000 years. (iii) The North American and Eurasian ice sheets advanced southward with rates well above 100 m/yr during the penultimate glacial inception and over 70 (Eurasia) and 90 (North America) m/kyr during last glacial inception. (iv) the Laurentide and Cordilleran ice sheets merge in their northern sectors in 13 out of 14 NROY simulations for MIS 7d, contrary to what is assumed from limited geological data. (v) larger ice sheets display a larger lag in the timing of stadial maximum ice volume compared to that of the insolation minimum; the North American ice sheet maximum lags 5.3 ± 0.5 kyrs behind the MIS 7d insolation minimum. Supplemental resources include a dynamic display of ice advance and subsequent retreat for a sub-ensemble of 14 NROY simulations from MIS 5d-5c and MIS 7d-7c.

1 Introduction

On the basis of stacked benthic δ^{18}O sea level proxies, glacial inceptions are characterised by relatively fast transitions from interglacial to glacial conditions and a rapid drop of sea level. This is clearly evident in the inferred up to 60 m eustatic sea

https://doi.org/10.5194/egusphere-2025-495
Preprint. Discussion started: 18 February 2025

level (mESL) drop during last glacial inception Marine Isotope Stages (MIS) 5e to 5d and even more clearly in the up to 80 mESL drop during the penultimate glacial inception, MIS 7e to 7d, over the course of approximately 12 kyrs (Spratt and Lisiecki, 2016, although different inferred sea level records display a range of possible ice evolution). However, the associated rapid growth in terrestrial ice volume has been difficult to replicate by Earth system models (e.g. Calov et al., 2005; Bahadory et al., 2021). The subsequent strong interstadial and associated sea level rise imposes a further challenge for both modeling and understanding. As such, glacial inceptions and subsequent interstadials offer a potentially powerful test of whether the net feedback response of an Earth systems model (ESM) to radiative forcing is of appropriate magnitude, a key issue for building confidence in modeling future climate evolution. This relates to a broader motivation for testing Earth system models under paleo boundary conditions: the extent to which underlying state dependence of current ESM configurations might invalidate their predictive ability for simulating ongoing and future climate change. For the context herein, this issue can be addressed concretely as the extent to which the capture of a single glacial inception by an ESM correlates with its capture of a different glacial inception, and furthermore, the extent to which the capture of present-day climate correlates with the capture of ice and climate over glacial inception.

The resolving power of the above test is dependent on the reliability of relevant paleo constraint data, which are especially scarce prior to the Last Glacial Maximum (LGM). Alternatively, existing stacked sea level records can provide insights into global ice volume changes, however they are subject to significant (often unquantified) uncertainties. Sea level estimates rely on δ^{18}O records, a convolution of eustatic sea level and deep ocean temperatures. A further source of uncertainty is the reliance on orbital tuning for the pre-^{14}C dating range. Four sea level records (Grant et al., 2014; Spratt and Lisiecki, 2016; Medina-Elizalde, 2013; Bates et al., 2014) published with uncertainty bounds are shown in Figure 1. Significant disagreements exist between the two, especially for the penultimate glacial cycle and both inceptions. Far-field and isotopic sea-level proxy records, moreover, can't offer information regarding the ice volume distribution between different ice sheets. Geomorphological data that could inform about individual ice sheet extent have very limited age control pre-^{14}C dating range. Furthermore, geological and geomorphological pre-LGM records are scarce since LGM ice overwrote most regions subject to episodic glacial cover during the Late Pleistocene.

A key ongoing challenge for paleoclimate modeling is computational cost. This challenge is addressed by invoking various approximations that limit accuracy. Uncoupled steady-state experiments (climate- or ice-only) lack key feedbacks and they therefore are not able to capture expected rates of sea level change (Khodri et al., 2001; Yoshimori et al., 2002; Vettoretti and Peltier, 2003; Otieno and Bromwich, 2009; Born et al., 2010; Colleoni et al., 2014). Early transient simulations of the entire last glacial cycle used two-dimensional energy balance or quasi-geostrophic climate models coupled to simple two or three-dimensional ice sheet models (Gallée et al., 1992; Peltier and Marshall, 1995; Tarasov and Peltier, 1997). While these models could capture the overall structure of ice growth and decay, they were unable to capture the minimum ice volume required to explain proxy-based inferences for the last glacial inception sea level low-stand. More recent work has employed Earth system models of intermediate complexity (EMICs) coupled to ice sheet models. Such studies to date that tested inception and subsequent ice retreat did not include an interactive Antarctic ice sheet. Most such studies also have significant discrepancies between simulated and geologically-inferred ice extent. For example, Alaska tends to be nearly fully ice-covered

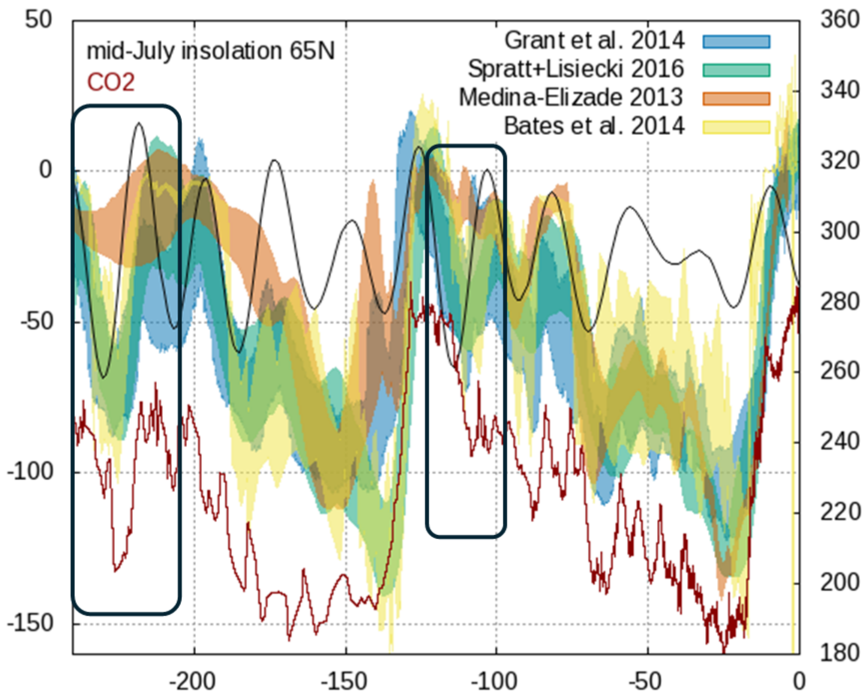

Figure 1. Sea level records (Grant et al., 2014; Spratt and Lisiecki, 2016; Medina-Elizalde, 2013; Bates et al., 2014), insolation (Laskar et al., 2004) and atmospheric CO_2 (Bereiter et al., 2015) for the last two glacial cycles. Black boxes indicate periods of interest in this study.

(e.g. Bahadory et al., 2021; Bonelli et al., 2009; Willeit et al., 2023) contradicting geological records (Kauman and Manley, 2004; Kaufman et al., 2011). Meanwhile, there is often not enough ice simulated over Quebec and Eurasia (EA) (e.g. Bonelli et al., 2009; Ganopolski et al., 2010, at least for LGM where geological data is available for comparison). Many models either poorly resolve critical feedbacks such as orographic forcing of precipitation (e.g. Bonelli et al., 2009; Ganopolski et al., 2010; Choudhury et al., 2020; Willeit et al., 2023) and/or simply lack feedbacks such as dynamic freshwater routing (e.g. Ganopolski et al., 2010; Bonelli et al., 2009; Choudhury et al., 2020).

The most successful attempts at simulating full glacial cycles with EMICs have to date relied on dust forcing (Ganopolski et al., 2010) or feedback (Willeit et al., 2023) to trigger ice retreat or keep areas ice-free. However, it remains unclear to what extent a reliance on dust forcing and or feedbacks is compensating for limitations in the utilized EMIC (the CLIMBER-2 EMIC used in Ganopolski et al., 2010, lacks a dynamical atmosphere). Dust process modeling is also subject to large uncertainties as regional dust input into the atmosphere and subsequent deposition is highly sensitive to regional aridity, winds, and turbulence. These characteristics are challenging for any EMIC to confidently capture. Atmospheric dust processes are therefore a potentially important but poorly constrained forcing and feedback.

Climate models have order 100 poorly constrained parameters (though for simpler EMICs many of these parameters are implicit). Furthermore, any computational model of a complex geophysical system will have significant trade-offs between fits to different tuning targets in parametric tuning. As such, analyses based on just one or a few model simulations provide a limited and sometimes unreliable basis on which to make climate predictions. We therefore present a perturbed-physics ensemble of transient simulations of the last two glacial inceptions and subsequent interstadials (MIS 5e to MIS 4 and MIS 7e to MIS 6e) with the fully coupled ice/climate model LCice. The latter interstadial inclusion is important to ensure that an adequate simulation of glacial inception is not due to a cold bias in the model. We combine geological knowledge and model results to analyze the evolution of the last two glacial inceptions. This includes comparing the simulated ice advance and maximum and minimum ice sheet extents with available geological data.

The LCice model is described in Section 2.1. Section 2.2 lays out the experiment setup. In climate modeling, capturing present-day climate appropriately is often implicitly assumed to provide predictive confidence. In Section 3.1, we explicitly test this assumption for different interglacial/glacial stages during the penultimate and last glacial inception. In Section 3.2, we present the phase relationships between insolation and ice sheet response in ice volume and area. Sea level stacks are usually orbitally tuned, using a poorly constrained insolation-δ^{18}O lag parameter (Lisiecki and Raymo, 2005). Modeling enables an independent assessment of the impact of orbital tuning. Section 3.3 examines the simulated ice evolution over the last two glacial inceptions with a focus on the maximum extent at MIS 7d and 5d and the differences and similarities between them. Animations of ice sheet evolution are available (https://doi.org/10.5446/69809 and https://doi.org/10.5446/69808). We compare the available geological data against our simulations, and consider what insights the simulations can provide where there is limited geological information. Section 3.4 considers inter-ensemble variability and the extent to which different ice sheet configurations are possible with the same simulated sea level change. Finally, we discuss and summarize our findings in Section 4.

2 Methods

2.1 The Model LCice2.0

LCice (visualized in Figure 2) consists of 3 components of the LOVECLIM model, including the atmosphere (ECBilt), ocean (CLIO) and vegetation (VECODE), coupled to an ice sheet systems model (GSM). LCice is forced by orbital parameters and greenhouse gas chronologies (Bereiter et al., 2015). LOVECLIM is an Earth system model of intermediate complexity (EMIC) capable of about 2.5 kyrs in 24 h on a single processor core with 4 x acceleration. LOVECLIM and its performance are discussed in detail by Goosse et al. (2010).

To enable interpretation of the simulation results, it is necessary to evaluate the strengths and weaknesses of the model. The key limitations are a combination of simplified process representation and limited spatial resolution. The vegetation component VECODE has only 3 classes: trees, grass and deserts; however, the Saharan desert is hard-coded in and cannot change to a vegetation type. The atmosphere ECBilt is quasi-geostrophic, on a T21 grid with 3 vertical levels. This means the model is suitable for capturing large (synoptic) scale mid-latitude atmospheric circulation but can’t resolve small-scale, tropical or mesoscale convective systems. The limited spatial resolution of ECBilt will also significantly affect its ability to capture atmospheric stationary wave dynamics over EA due to NA ice sheet forcing, as well as associated changes in precipitation (with

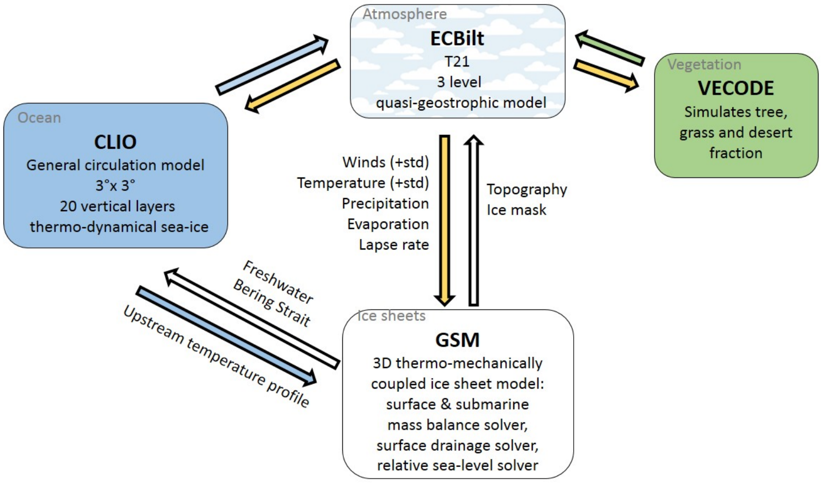

Figure 2. LCice components and couplings

storm track displacement) and the amplitude of the seasonal cycle. In a suite of grid resolution sensitivity tests with the CAM3 atmospheric GCM (with full LGM boundary conditions) forcing an ice sheet model, Lofverstrom and Liakka (2018) find that T42 is the minimum resolution to grow inferred LGM EA ice extent though LGM NA ice extent can be reasonably captured at T21 (except for excessive glaciation of Alaska, which is not present in the T31 simulation). Goosse et al. 2010 find for default parameter values that LOVECLIM captures the present-day surface temperature pattern and the magnitude of precipitation of the mean climate “reasonably well” compared to observations appropriately smoothed to LOVECLIM resolution. However, a warm temperature bias exists in the tropics and the eastern Pacific, and the precipitation pattern is too symmetric between Northern and Southern Hemispheres. The extent of LGM annual mean cooling in LOVECLIM is in approximate agreement with other PMIP2 models (Goosse et al., 2010).

The ocean component CLIO is relatively complex compared to other EMICs. It is a full general circulation model (rather than e.g. the frictional-geostrophic model in the relatively new CLIMBER-X Willeit et al., 2022). The model simulates the magnitude of the meridional overturning circulation in agreement with observations (Goosse et al., 2010). However, the 3°x 3°grid is too coarse to adequately resolve ocean circulation under ice shelves, and current Antarctic ice shelves are represented as land rather than ocean grid cells. Furthermore, the land-sea mask and bathymetry (except for the Bering Strait throughflow) are time-independent in the model and fixed to present-day conditions. Although sea level changes, no ocean cells can be turned into land cells (or vice versa). To partially compensate, LCice has a sea level dependent parametrized Bering Strait through-flow in the ocean model.

The pre-existing LOVECLIM components are coupled to the Glacial Systems Model GSM (Bahadory and Tarasov, 2018). The coupler includes all important feedbacks between climate and ice for a glacial cycle context (Figure 2) except potentially dust (Willeit et al., 2022). It passes the monthly mean and standard deviation of temperature and monthly means of wind, precipitation, evaporation and lapse rate from ECBilt to the GSM. The downscaling scheme accounts for the orographic forcing of precipitation on the higher-resolution GSM grid. The temperature downscaling uses the LOVECLIM vertical atmospheric temperature gradient (lapse rate Bahadory and Tarasov, 2018). The GSM passes the ice mask and topography to the atmosphere, and a model parameter controls the topographic upscaling scheme (simple, envelope, or silhouette) from high to low-resolution grids. Furthermore, the GSM computes and passes topographically consistent freshwater fluxes to CLIO. Conversely, CLIO passes ocean temperature profiles to the GSM to calculate the submarine melting of marine-terminating ice sheets and ice shelves.

Since the first publication using LCice (Bahadory and Tarasov, 2018), we have updated the coupler, the most significant update of which is the inclusion of a dynamic Antarctic ice sheet. The GSM has also been updated, including the conversion from pure shallow ice approximation to hybrid shallow ice/shallow shelf ice dynamics, and the introduction of a novel (and physically motivated) accounting for the impact of changing insolation forcing on surface mass-balance (Tarasov et al., in prep.).

A further significant change from Bahadory and Tarasov (2018) is the addition of temperature and precipitation bias corrections. Previous modeling efforts (Vettoretti and Peltier, 2003; Ganopolski et al., 2010; Willeit et al., 2023) have shown that model biases can have a significant impact on glacial cycle modeling. A key challenge is that there is no basis for assuming that present-day model biases would persist in total over a glacial cycle. Therefore, the bias correction used here decreases with increasing ice volume. At LGM sea level, the correction is 0, and at PD sea level, the full correction is applied. The transition between these states depends on a parameter value. For each different LOVECLIM parameter vector, the corresponding base-line bias correction is set to the present-day monthly-mean discrepancy between simulation and 1980-2000 CE ERA 5 climatology (Hersbach et al., 2020).

Since precipitation patterns will likely change much more drastically than temperature, the precipitation bias correction is imposed as a monthly scalar from the present-day continental scale spatial mean anomaly. To address the common problem of excessive ice advance over Alaska and Siberia, which would otherwise distort results for adjacent regions, (e.g. Bahadory et al., 2021), we impose further ad-hoc temperature increases in these two regions (ranging from $+1$K to $+9K$).

Given the possibility of inadequate capture of radiative feedbacks in LOVECLIM, we have also added a greenhouse gas radiative factor ensemble parameter, as suggested by Choudhury et al. (2020). The factor increases the atmospheric radiative sensitivity to CO_2 variations with respect to the reference CO_2 value and ranges from 1.5 to 2.5. In total, every ensemble member has a parameter vector of 18 LOVECLIM and 23 GSM parameters that are varied.

2.2 Experiment Setup

We use fit to present-day (PD) climate to select initial LCice parameter vectors for glacial inception simulations. To do so, plausible prior distributions for 18 LOVECLIM parameter values were defined. 2000 different LOVECLIM parameter vectors were then selected via Latin-hypercube sampling from these distributions. For each parameter vector, LOVECLIM was started with PD initial conditions at 1200 years before present and runs transiently uncoupled for 1 kyrs before activating coupling to the GSM.

We filter the simulations by comparison against ERA 5 (Hersbach et al., 2020) and ORAS 5 (Copernicus, 2021) reanalysis for the mean of 1980-2000. The metrics chosen for filtering are based on their importance for ice sheet growth and decay (summarized in Table 1). The metrics are as follows. 1) Mean 2 m temperature seasonality (June, July, August - December, January, February; JJA-DJF). This is motivated by the assumption that an ensemble member with the appropriate sensitivity to seasonal insolation cycling is also more likely to display the right sensitivity to insolation changes on glacial cycle time scales. 2) Mean annual precipitation, which is essential for ice sheet accumulation. 3) Southern Ocean temperature, which is important for Antarctic sub-shelf melt. Metrics 1 and 2 are evaluated over areas where ice sheet advance is expected during inception, such as Northern Canada (North America North, NAN), Hudson Bay region (North America South, NAS), West Eurasia (EAW), West Antarctic Ice Sheet (WAIS), and East Antarctic Ice Sheet (EAIS); and in regions inferred to remain ice-free despite their high latitudes such as Alaska (NAAL) and Eastern Eurasia (EAE).

Ensemble members that simulate metrics within 4 sigma time variance of ERA 5 make up the not-ruled-out-yet (NROY) ensemble subset. We chose a 4-sigma range to partially compensate for limited sampling and an incomplete error model. The PD NROY ensemble subset narrows the parameter value ranges from which we resample to create a new ensemble to repeat the filtering process. In the end, 90 LCice parameter vectors result in simulations that pass the filtering process and are used for the last glacial inception simulations. The mean of the sub-ensemble that we will analyze later on (14 inception NROY ensemble members) shows a pronounced cold bias over the Arctic Ocean and a warm bias over North America (NA) winter for PD Figure A1). These biases are much weaker in summer, however a warm bias over Labrador and Northern Siberia (ice inception areas) persist. In both seasons, there is a cold bias over West Antarctica and a warm bias over East Antarctica. Precipitation biases are most substantial in small-scale, high-elevation areas and the tropics. In northern hemisphere ice sheet regions, LCice displays a light wet bias over NA (except for the coastal mountain area) and a light dry bias over Scandinavia. Although far from complete, these biases give a crude initial estimate of the structural uncertainty of the model if one assumes that persistent biases proportionally reflect underlying model limitations.

The ensemble for each of the last and penultimate glacial inceptions consists of 90 PD NROY parameter vectors. Penultimate glacial inception simulations start at 240 ka, last glacial inception at 122 ka. Sea level records suggest that the last (penultimate) interglacial likely had a higher (lower) than PD sea level. As the exact configuration of the Greenland and Antarctic ice sheets of the interglacial has high uncertainties, we opted to use the well-known PD conditions for initializing simulations for both time-frames. LOVECLIM is first spun up for 2 kyrs uncoupled at constant 240 ka (122 ka) forcing. Then the GSM is spun up for 7 kyrs using the LOVECLIM 240 ka (122 ka) climate before full ice/climate coupling is activated. Choudhury et al. (2020) use LOVECLIM at 5 x acceleration and found that the ice sheet evolution is relatively insensitive to reduced acceleration. We choose a slightly more conservative 4 x acceleration in this study.

Table 1. NROY (not ruled out yet) conditions for a subset of best ensemble members. Areas of evaluation are displayed in Figure A2

Metric	Area	Filter criteria PD	Filter criteria MIS 7d	Filter criteria 5d	Filter criteria MIS 7c	Filter criteria MIS 5c
Mean 2m-temperature JJA-DJF 1981-2000	North America (NAN, NAS, NAAL), Eurasia (EAW, EAE), Antarctica (WAIS, EAIS)	4σ ERA 5 reanalysis time variance	-	-	-	-
Mean annual precipitation 1981-2000	North America (NAN, NAS, NAAL), Eurasia (EAW, EAE), Antarctica (WAIS, EAIS)	4σ ERA 5 reanalysis time variance	-	-	-	-
Mean ocean temperature profile 1981-2000	Southern Ocean	70 % in 4σ ORAS 5 reanalysis time variance	-	-	-	-
Sea level	global	-	eustatic sea level lower than 25 m relative to PD between 240 - 210 ka	eustatic sea level lower than 20 m relative to PD between 115 - 105 ka	decreased sea level compared to MIS 7d	decreased sea level compared to MIS 5d

3 Results

Given the model limitations outlined in Section 2.1, the simulation results should not be interpreted as reconstructions. However, there is arguably inferential value in selective characteristics of ice sheet evolution consistently observed across the NROY ensemble.

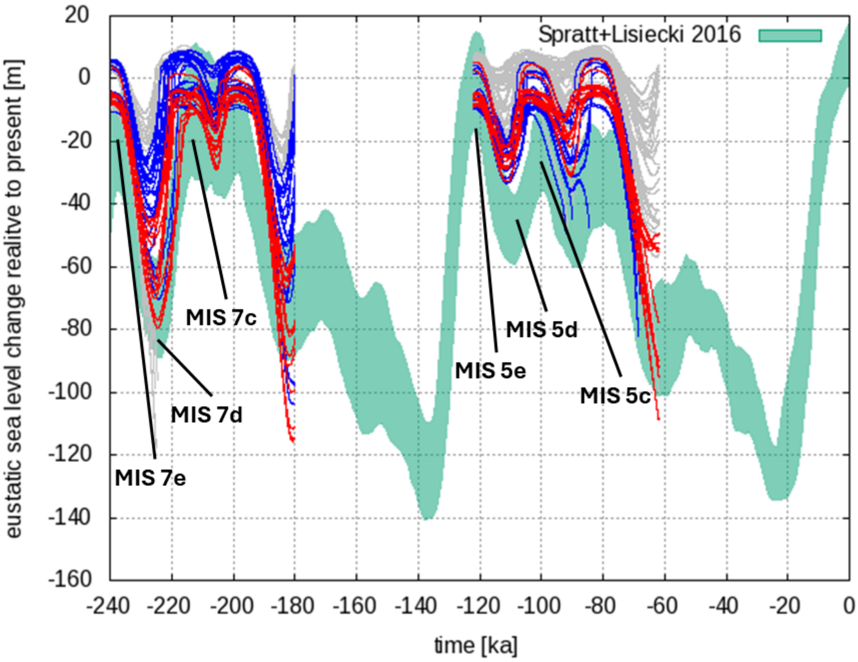

Figure 3. Sea level reconstruction in green (Spratt and Lisiecki, 2016) and simulated sea level change for the 2 full ensembles of the penultimate and last glacial cycle. Grey: all ensemble members (which are NROY for present-day constraints), blue: ensemble members that passed filtering for either only MIS 7d/c or MIS 5d/c, red: 14-member NROY sub-ensemble

In the following, we analyze the simulations with respect to global eustatic sea level change (Section 3.1), mean phasing of ice volume and area with insolation (Section 3.2), and ice area and geometry compared to geological and geomorphological evidence (Section 3.3).

3.1 Simulated Sea Level Performance

The two glacial inception ensembles are filtered for sea level high and low stands based on the combined information of the sea level stacks displayed in Figure 1. Ensemble members are ruled out if their simulated sea level minima does not reach at least 25 m at MIS 7d and 20 m at MIS 5d. Furthermore, ensemble members need to display an increased sea-level from MIS 7d to MIS 7c and from MIS 5d to MIS 5c. Only 14 ensemble members pass the sea level filter (red in Figure 3), embodying the inception NROY sub-ensemble we analyze below.

The hypothesis that reasonable performance for PD climate predicts reasonable performance for glacial inception is not supported, as seen from the wide range of grey-coloured simulations in Figure 3. Furthermore, an ensemble member that performs well for the last glacial inception does not necessarily perform well for the penultimate glacial inception and vice versa (blue in Figure 3). 38 of the 90 simulations pass the sea level filter for MIS 7d only, 29 for MIS 5d only. All ensemble members that pass for MIS7d/5d decrease in ice volume after the sea level low stand and therefore pass the filtering criteria for

Table 2. Ensemble mean maximum growth and retreat rates for ice sheet volume (in sea level equivalent) and area (at the southern)for MIS 7d and 5d.

MIS	Volume growth rate NA [mSLE/kyr]	Volume growth rate EA [mSLE/kyr]	Volume melt rate NA [mSLE/kyr]	Volume melt rate EA [mSLE/kyr]	Southern margin growth rate NA [m/kyr]	Southern margin retreat rate NA [m/kyr]	Southern margin growth rate EA [m/kyr]	Southern margin retreat rate EA [m/kyr]
MIS 7d	4.6 ± 1.0	2.6 ± 0.9	9.7 ± 7.6	4.1 ± 5.8	168 ± 35	28215 ± 10747	158 ± 45	339 ± 98
MIS 5d	3.0 ± 0.5	1.3 ± 0.5	6.8 ± 4.3	0.8 ± 1.4	97 ± 35	14312 ± 13821	73 ± 84	961 ± 796

MIS 7c/5c. The overlap of members passing for each stage results in only 14 remaining ensemble members (red in Figure 3). MIS 5d sea level poses the strongest constraint on the ensemble.

The NROY sub-ensemble shows that the NA ice sheet (combined Innuitian, Cordillerian, and Laurentide ice sheets) grew and melted ice volume faster than the EA ice sheet. During the NROY ensemble mean growth interval from MIS 7e to MIS 7d a maximum growth rate over 4 mSLE/kyr (meters of sea level equivalent per 1000 years) and melting rates of over 9 mSLE/kyr between MIS 7d and MIS 7c are reached (see Table 2). The ensemble mean EA ice sheet reached a maximum growth rate of over 2 mSLE/kyr during the growth towards MIS 7d and 4 mSLE/kyr of mass loss following the MIS 7d ice volume maximum. The ensemble standard deviation is large for the retreat rates, indicating a high variability not just in retreat rate but also in timing of maximum retreat.

Glacial inception performance is not attributable to individual parameter values. We tested attribution via the mean cosine angle as a measure of similarity between the NROY parameter vectors within the sub-ensemble of members passing MIS 7d-7c filters, members passing MIS 5d-5c filters, and members passing both. No similarity is found within any of the ensemble subsets. This suggests that non-linearities between the interactions of the different parameters are at play and cannot be disentangled here. The only constraint established here for capturing the last two glacial inceptions is a greenhouse gas radiative factor between 2.0 and 2.5 (following Choudhury et al. (2020), tested values were 1.5, 2.0, and 2.5). All varied parameters and their value range can be found in Table B1.

3.2 Phasing of Ice Sheet Volume and Area

To determine the phase relationship between ice area, volume and insolation, and differences in the phasing between the last two glacial inceptions, the inceptions are aligned by their insolation minima and maxima in Figures 4 and 5 (black line for penultimate, grey line for last glacial; note the two time axes corresponding to penultimate glacial inception on the bottom and last glacial inception at the top).

Table 3. Timing of insolation minimum and ice area and volume maximum

MIS	insolation min.	NA ice area max.	EA ice area max.	NA ice volume max.	EA ice volume max.
MIS 7d	230 ka	226.2 ± 9.6 ka	227.9 ± 4.4 ka	224.7 ± 1.6 ka	227.6 ± 0.5 ka
MIS 5d	114 ka	112.8 ± 6.2 ka	113.7 ± 2.0 ka	110.6 ± 0.7 ka	113.5 ± 0.2 ka

The NA ice sheet (blue shades on left panel in Figures 4 and 5) is substantially larger than the EA ice sheet (orange shades on left panel in Figures 4 and 5) throughout the last two glacial inceptions. NA and EA are larger during the penultimate inception than during the last glacial inception.

In accord with the relative direct control of maximal ice extent by summer temperature and insolation, the ice area maximum has a small lag behind the summer insolation minimum for the Northern hemisphere ice sheets (see Table 3).

The ice volume maximum lags further behind the ice area maximum. Willeit et al. (2023) find a similar behaviour in their simulations: the ice sheets expand thinly at first, then the ice thickens. Ice thickening compensates for the early area retreat so that the maximum ice volume can be reached after the maximum ice area. This lag of maximum volume behind maximum area is not apparent for EA inception, but significant for the larger NA ice complex (2.2 kyrs at MIS 5d, 1.5 kyrs at MIS 7d, Table 3). A strong correlation between ice volume and time lag of ice volume behind insolation forcing is especially evident for NA MIS 5d and 7d (see Figure 6). In accordance, the smaller EA ice sheet reaches its maximum volume before the NA and shows less lag between maximum ice volume, maximum ice area and minimum insolation.

The Greenland ice sheet's lag of up to 7 kyr behind the insolation minimum during MIS 7d does not match the corresponding relationship for the more ice-volume proximal EA ice sheet in Figure 6 (black symbols). Instead, its lags approximate match those of the much larger NA ice sheet. We reason that the fast response of the EA ice sheet compared to the NA and Greenland ice sheets to insolation forcing is mainly due to the increased ratio of potential ablation relative to accumulation as quantified by the larger ice margin length to ice sheet area ratio. Furthermore, for the majority of simulations, the EA ice sheet is not one coherent ice sheet. Instead, it consists of a minimum of 3 distinct ice sheets with extensive marine margins that can migrate more quickly than terrestrial margins. Finally the downstream proximity of NA to Greenland implies that the climate response to a large NA ice sheet will also strongly affect Greenland. The factors also likely explain the somewhat larger sub-ensemble variance in the timing of the EA ice sheet area and volume peaks compared to that of the NA ice sheet.

The Antarctic ice sheet, contrary to the Northern Hemisphere ice sheets, remained at a relatively constant area and volume. This may be due to the present-day tuning of subshelf ocean temperature bias corrections for Antarctica as well as limitations in the GSM subshelf melt model. During the penultimate inception (dark blue on right panel in Figure 4, the Antarctic ice volume and area show a small reduction at 217 ka. This coincides with the highest southern hemisphere summer insolation during the last two glacial cycles (551 W/m^2), which caused the WAIS to retreat.

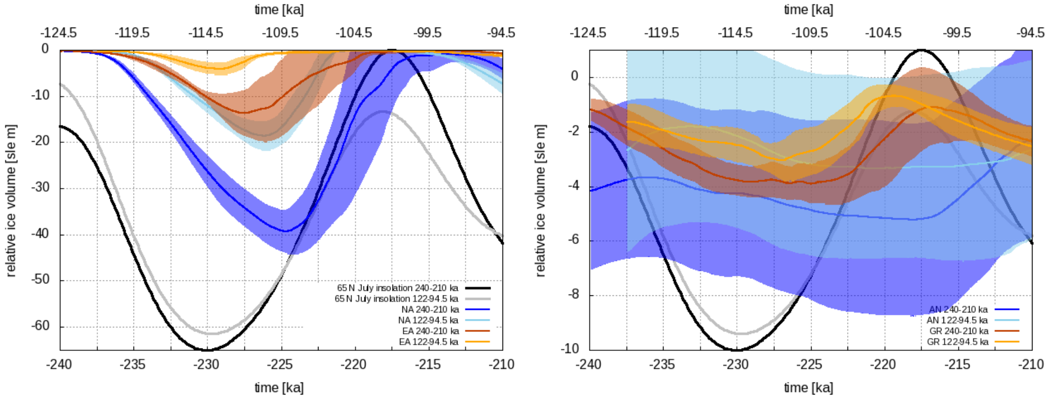

Figure 4. mean and standard deviation of NROY ensemble ice volume as sea level equivalent for NA and EA (left) and Greenland and Antarctica (right). Note the top and bottom time axis, aligning July insolation peaks at 65 N for the last two glacial inceptions.

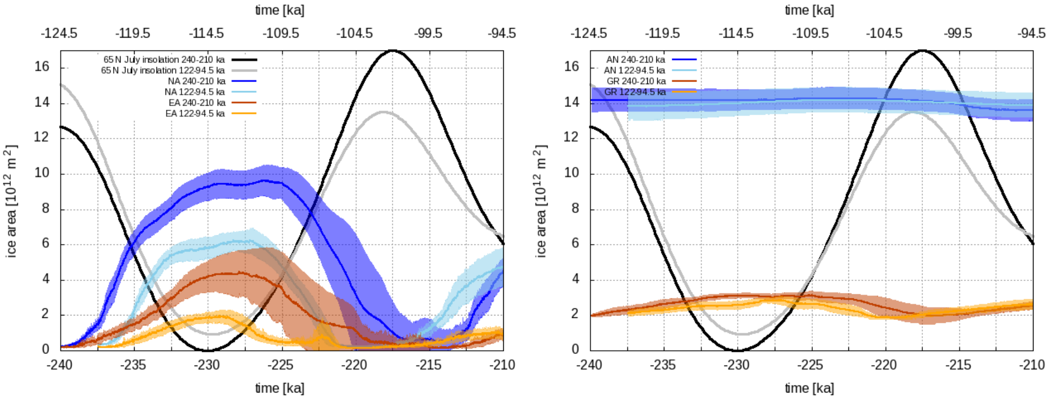

Figure 5. mean and standard deviation of NROY ensemble ice area for NA and EA (left) and Greenland and Antarctica (right). Note the top and bottom time axis, aligning July insolation peaks at 65 N for the last two glacial inceptions.

3.3 Evolution of extent, location and geometry of the Eurasian and North American ice sheets

While the present-day existing Greenland and Antarctic ice sheets grew during the last two glacial cycles, their advance was spatially restricted by the marine bordering landmasses. Therefore, we focus solely on the EA and NA ice sheets in this section. For a dynamic display of ice advance and decay of all 14 members from MIS 5d-5c and MIS 7d-7c, see https://doi.org/10.5446/69809 and https://doi.org/10.5446/69808.

In simplified 0-dimensional modeling, temperature is often used to drive ice sheet margin position. The ensemble simulations show that there is a relationship between ice margin and isotherms, depending on state of the ice sheet. During the inception advance of the NA ice sheet, the simulated southern ice margin approximately aligns with the summer -2°C isotherm (specifically mean June-Aug, JJA, at sea level) in most regions (Figures B1 - B12). At maximum extent, the ice margin lies

https://doi.org/10.5194/egusphere-2025-495
Preprint. Discussion started: 18 February 2025

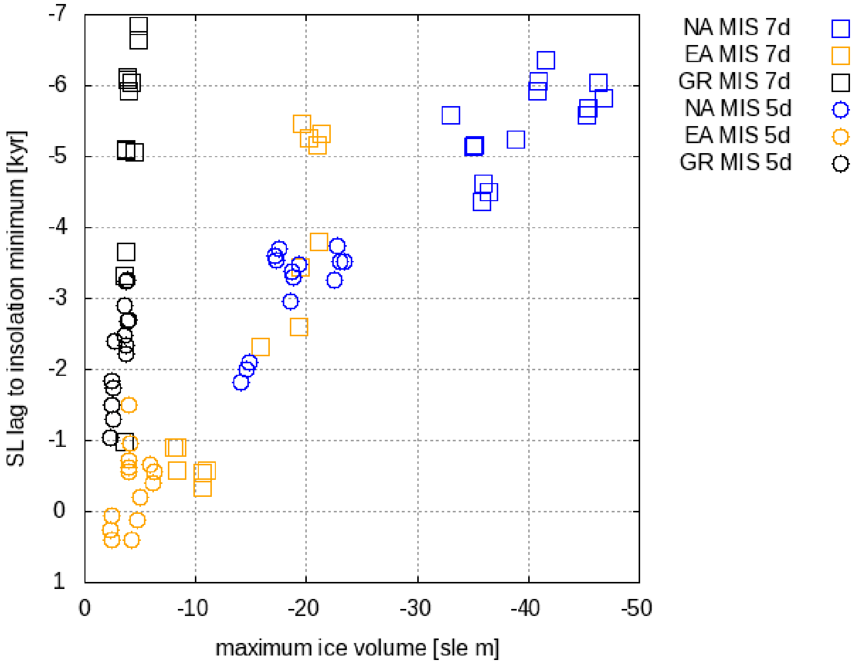

Figure 6. NA (blue), EA (orange), and Greenland (black) maximum ice volume for each of the 14 NROY ensemble members at MIS 5d and MIS 7d and the according time lag between insolation minimum and timing of ice volume maximum

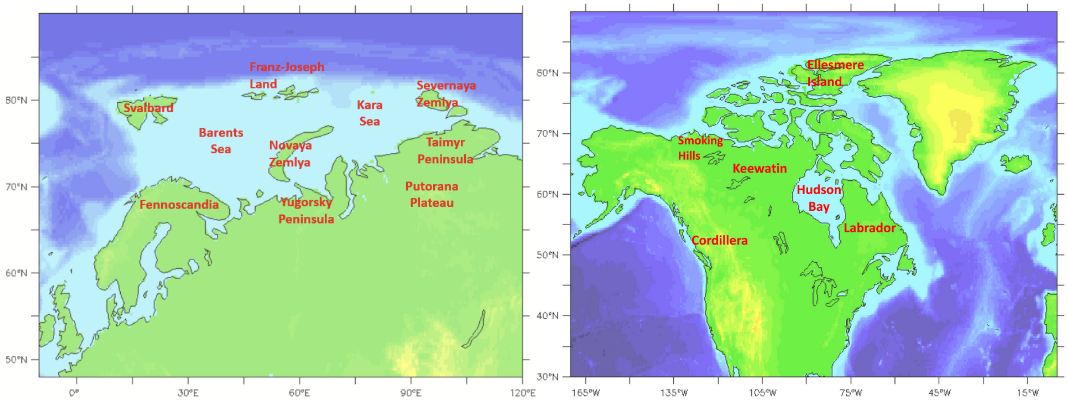

Figure 7. Overview of the study areas and names mentioned in EA (left) and NA (right)

between the -2 and 0°C JJA isotherm. During the retreat phase, the ice margin aligns with or is south of the 4°C JJA isotherm. This warmer isotherm during retreat is in accord with the varying combinations of thicker marginal ice and higher marginal ice flux during retreat. Ice margins of mountainous regions like the Cordilleran lie south of the aforementioned isotherms, as the isotherms are evaluated at sea-level. The EA ice sheet has more extensive marine margins during advance and retreat phases and even during MIS 5d. For these, the simple relationship between ice margin and summer air temperature does not hold given the impact of calving and submarine melt. For the continental margins during MIS 7d ice advance, the same relationship as for the Laurentide ice sheet holds; the ice margin lies between the -2 and 0°C isotherm.

3.3.1 The onset of glaciation: Eurasian ice growth from simulation start to MIS 7d and 5d

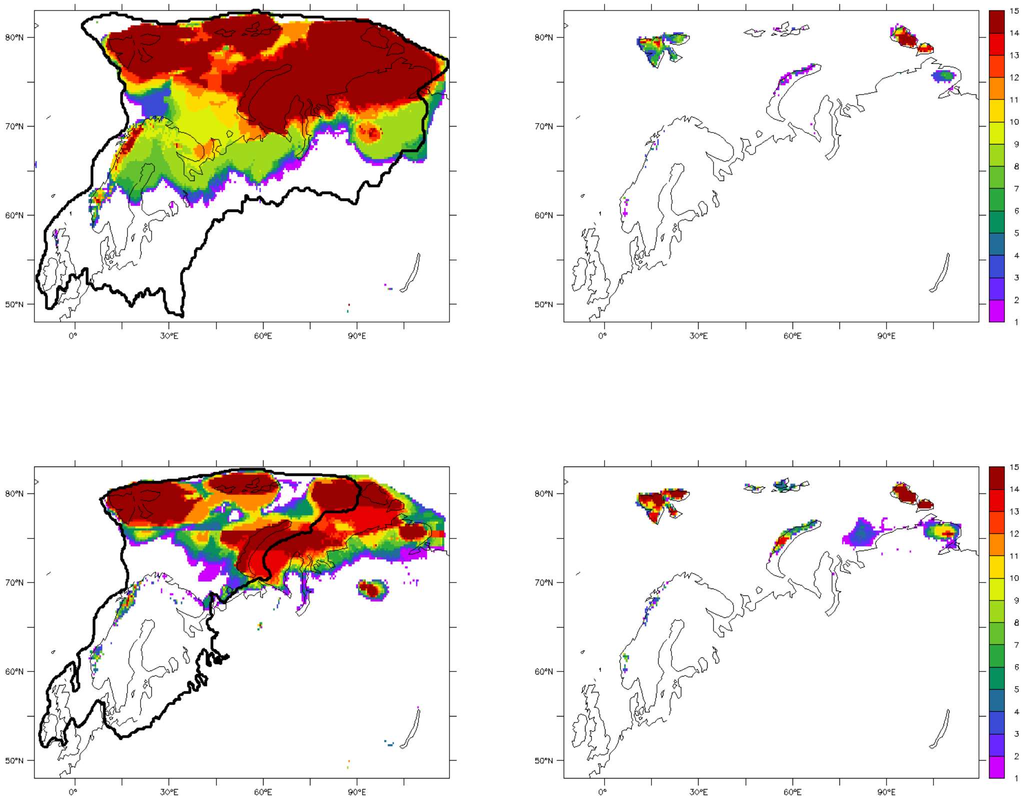

Figure 8. Density plot of maximum ice sheet extent over EA at MIS 7d (top left) and MIS 5d (bottom left) and minimum ice sheet ectent at MIS 7c (top right) and MIS 5c (bottom right). The colour indicates the number of NROY ensemble members (out of 14) simulating ice over the area. The bias correction over Alaska and Siberia can lead to "artificially" straight boundaries. Black contour lines give a maximum extent estimate. Due to a lack of maximum extent estimates for inception, the glacial maximum extent is displayed: for MIS 7d, the Saalian maximum extent from Svendsen et al. (2004) as an upper limit; for MIS 5d, the LGM ice sheet extent from Hughes et al. (2016).

At onset, the EA ice advance in the simulations begins over areas where ice persists to present-day, including Svalbard, Franz-Joseph Land, and Severnaya Zemlya (see locations in Figure 7 and dynamic ice advance in https://doi.org/10.5446/69809 and https://doi.org/10.5446/69808). The ice then expanded beyond the present-day landmasses from the islands into the Barents and Kara Sea. The southernmost margin advanced on average 73 ± 84 m/yr southward from MIS 5e-d and 158 ± 45 m/yr from MIS 7e-d (see Table 2). Following this initial onset of glaciation, the differences between MIS 7d and MIS 5d become evident, as described below.

MIS 7d: This southward spread of ice was more pronounced during MIS 7d, where the maximum ice area was reached at 227.9 ka in the NROY simulations. All ensemble members have some ice in the Scandinavian Mountains. 50 % of members have ice cover over the northern half of Fennoscandia and ice down to 65 N in the region of the Taymyr Peninsula (Figure 8, left).

Geological data constraining the MIS 7d interval of EA ice are sparse. Astakhov and Semionova (2021) describe marine records dated to MIS 7 in north-central Russia (Volma, Pupkovo settlement). Glaciomarine sediments from the Taimyr Peninsula have also been dated to MIS 7 (Möller et al., 2019a, b). However, age uncertainties for these geological data are, at minimum, ±16 ka, so it is unclear whether these sites date the onset of glaciation (as described in the simulations) or a time several kyrs before/after. These sites are all situated at or south of the simulated MIS 7d ice margin. More broadly, the simulated ice advance is significantly less extensive than what is suggested by the review work of Svendsen et al. (2004), who suggest that MIS 7 ice extended several hundred kilometers farther to the southwest than what is depicted in the simulation (Figure 8).

MIS 5d: The simulated southward spread of ice from glacial inception centres over EA was less pronounced during MIS 5d. The ensemble mean maximum ice area was reached at 113.7 ka. About 80 % of simulations have ice from Svalbard and Franz-Joseph Land merged, some ice in the north of Taymyr Peninsula, and a few spots in the Scandinavian mountains (Figure 8). All ensemble members have an additional ice dome in the Kara Sea. Ice was largely absent from the Russian and Fennoscandian mainland, with the exception of some small glacial areas in high-latitude areas of Norway. Geological data spanning MIS 5 are somewhat more abundant, however, precise constraints on the ice margin remain elusive. Geological investigations suggest that MIS 5d glacial initiation may have occurred in the Barents-Kara seas as well as on the Russian mainland, for example, on the high-elevation Yugorski Peninsula as well as the Putorana Plateau (Astakhov et al., 2016). The Barents-Kara ice sheet may have eventually spread southward, merging with the aforementioned ice masses on the Russian mainland as suggested by stratigraphic work from the Taimyr Peninsula, northern Russia and Fennoscandia, all of which have bracketed local ice advance during MIS 5d (Möller et al., 2019a, 2015, 2008). Geological data spanning MIS 5 are somewhat more abundant, however, precise constraints on the ice margin remain elusive. 290 Geological investigations suggest that MIS 5d glacial initiation may have occurred in the Barents-Kara seas as well as on the Russian mainland, for example, on the high-elevation Yugorski Peninsula as well as the Putorana Plateau (Astakhov et al., 2016). The Barents-Kara ice sheet may have eventually spread southward, merging with the aforementioned ice masses on the Russian mainland as suggested by stratigraphic work from the Taimyr Peninsula, northern Russia and Fennoscandia, all of which have bracketed local ice advance during MIS 5d (Möller et al., 2019a, 2015, 2008). Like the MIS 7c inceprtion, the simulated ice advance during MIS 5d is significantly less extensive than what is suggested by review work in the area (Hughes et al., 2016), who suggest that MIS 5d ice extended several hundred kilometers farther to the southwest than what is depicted in the simulation (Figure 8).

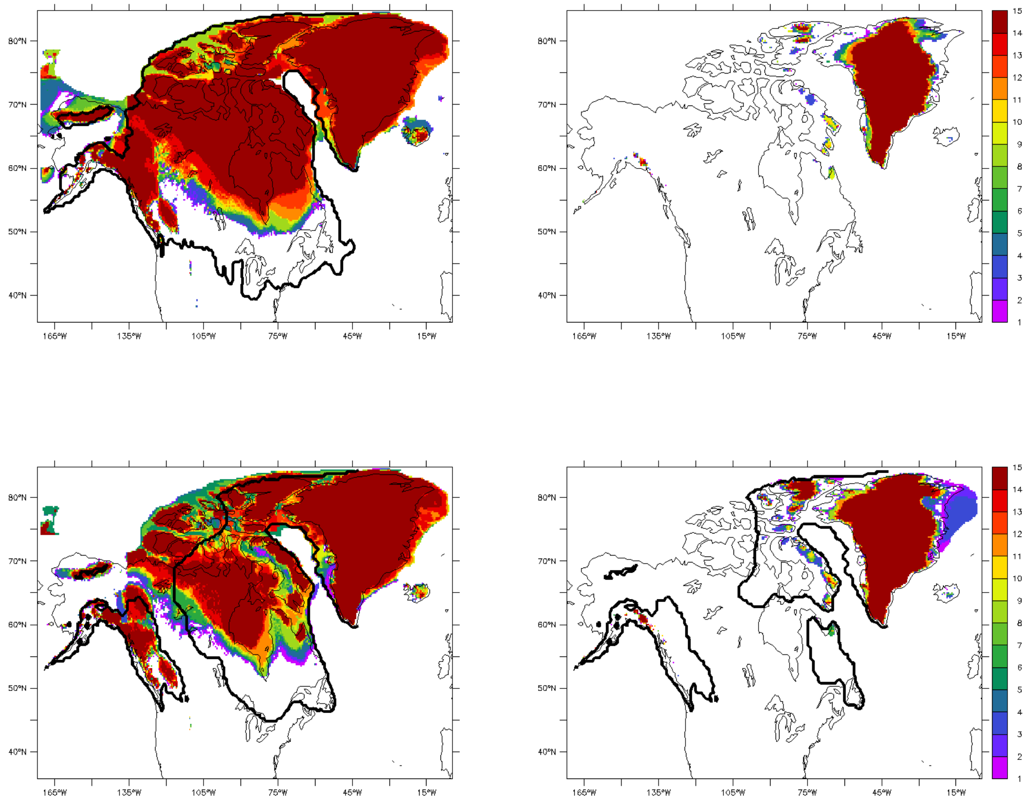

Figure 9. Density plot of maximum ice sheet extent over NA at MIS 7d (top left) and MIS 5d (bottom left) and minimum extent at MIS 7c (top right) amd MIS 5c (bottom right). The colour indicates the number of NROY ensemble members (out of 14) simulating ice over the area. The bias correction over Alaska and Siberia can lead to "artificially" straight boundaries. Black contour lines give a maximum extent estimate. Due to a lack of maximum extent estimates for NA during MIS 7d, LGM maximum extent reconstruction from Dalton et al. (2022) is displayed. For MIS 5d, the reconstruction for 110 ka from Dalton et al. (2022) is shown. For MIS 5c, the reconstruction for 100 ka from Dalton et al. (2022) is shown.

3.3.2 The onset of glaciation: North American ice growth from simulation start to MIS 7d and 5d

Glaciation in NA started on Ellesmere Island for all simulations consistent with the primary control of summer air temperature. From there, most simulations have ice subsequently advance over the Arctic Archipelago and Keewatin (see dynamic ice evolution in https://doi.org/10.5446/69809 and https://doi.org/10.5446/69808). A secondary controlling role for precipitation is partly evident in the few simulations that have additional nucleation over the much higher precipitation region of the Canadian Coastal Mountains.

The NA ice sheet advanced southwards rapidly, with NROY ensemble mean simulated advance rates of 97 m/yr at the southernmost margin during MIS 5e-d and 168 m/yr during MIS 7e-d with an NROY ensemble standard variation of ± 35 during both time periods. Following this initial onset of glaciation, some differences between MIS 7d and MIS 5d become evident, as described below.

MIS 7d:

In the simulations covering MIS 7d, the Keewatin Dome extended southward to approximately the boundary of the Canadian Shield and had a thickness of above 3 km (Figure 9, left). The maximum ice area is reached at 226.2 ka. During MIS 7d, all 14 NROY ensemble members simulate a completely ice-covered Hudson Bay and 13 out of 14 simulate a merged Cordilleran and Laurentide ice sheet in the northernmost sector. Hudson Bay can glaciate very fast (see gif in video supplements: https://doi.org/10.5446/69809 and https://doi.org/10.5446/69808). Ice appears first in the North of Hudson Bay, including the connection to Hudson Strait, after which the rest of Hudson Bay can glaciate within 2 kyr.

There are presently very few geological data constraining the MIS 7d ice advance over NA. Geological evidence from north-central Alberta does support an active Keewatin ice dome during several parts of the Quaternary (e.g. Andriashek and Barendregt, 2017), but these ice advances are not constrained to specific intervals. The only terrestrial records spanning that interval are located well outside the glaciated region and therefore offer no precise constraint on ice sheet advance (Cheng et al., 2019; Winograd et al., 1992). Nevertheless, it is possible to make some broad comparisons between the simulations and geological inferences. A recent review of the Smoking Hills area, lying adjacent to the MacKenzie River, suggests that the majority of glacial sediments in this area are from the last glacial maximum (∼25 k), while some of the oldest constrained via cosmogenic burial dating to an ice advance at 2.9 ± 0.3 Ma (Evans et al., 2021). Although these data constrain an ice advance significantly earlier than what is covered in this manuscript, they nevertheless support the presence of continental ice in this area prior to the LGM, and, presumably, the merging of the Cordilleran and Laurentide ice sheets at that time. The merging of these two ice sheets prior to the LGM is notable since the prevailing view is that they merged only at the LGM (see Discussion).

MIS 5d: The southward spread of ice from glacial inception centres over northern Canada is less pronounced during MIS 5d in the simulations. The maximum ice area was reached at 112.8 ka, and the simulated Keewatin ice sheet dome reached just below 3 km. During MIS 5d, 11 out of 14 ensemble members have Hudson Bay completely ice-covered (Figure 9, bottom left), and none fully merge the Laurentide and Cordilleran ice sheets.

An estimate of the maximum ice area for this interval (around 110 ka) has been compiled by Dalton et al. (2022), however the measure of confidence in this ice reconstruction is low owing to a shortage of geological constraints. Areas of agreement between the simulation and geological data include ice-free conditions in Atlantic Canada (Vernal et al., 1986; Rémillard et al., 2017). A major area of contrast between the simulations and the geological data is the relative size of the Labrador and Keewatin domes. However, it is important to keep in mind the geological outline in Figure 9 represented the maximum ice area for this interval (around 110 ka). Only 4 ensemble members have ice cover over Labrador, but all have ice cover over a large swath of Keewatin. Geologists, however, traditionally suggest glacial inception started in broad high-altitude areas of Northern Labrador owing to prolonged snow cover and increased precipitation (Ives, 1957; Koerner, 1980). This hypothesis is supported by glacial striae and flowlines indicative of a relatively early expansion of the Labrador Dome to almost the boundaries of the

Canadian Shield (Kleman et al., 2010). However, very little of this evidence for glacial inception is directly dated – instead, most is inferential or constrained using indirect dating methods. The lack of a geological inference for early glaciation over Keewatin may simply reflect the paucity of field data over the broad Keewatin area, though recently, more attention has been paid to mapping and geomorphic work in these areas (Campbell et al., 2013; McMartin et al., 2021, 2023).

The 50 % of ensemble members that grow ice over Labrador during MIS 5d also grow ice furthest south over Labrador during MIS 7d. The ensemble members are characterized by above-average precipitation east of Hudson Bay compared to the rest of the sub-ensemble. Ensemble members with a glacial lobe over Labrador display a retreat pattern where the Laurentide ice sheet retreats from west to east from MIS 7/5d to MIS 7/5c, with the ice over northern Quebec and Baffin Island remaining last. This is similar to that long geologically-inferred to have happened for the last deglaciation (e.g. Dyke, 2004). The rest of the ensemble retreats from all edges to the center, with the last ice remaining west of Hudson Bay.

3.3.3 Ice evolution through MIS 7c and MIS 5c

The substages c during MIS 7 and 5 have minimal geological constraint aside from maximum extent for EA MIS 5b. When available (which is rare, especially for MIS 7), geological data can't be confidently assigned to a specific substage. Moreover, records purporting to document ice extent (ie. striation data) are inferentially dated or constrained using indirect dating methods. For this reason, the discussion of geological data below is sparse.

Eurasia: During MIS 7c and MIS 5c, over EA, the simulated ice retreated to Svalbard and Severnaya Zemlya (Figure 8). The ice retreated on average 961 m/yr at the southern margin (with a high ensemble standard deviation of ± 796 m/yr) from MIS 5d to 5c and from MIS 7d to MIS 7c with 339 ± 98 m/yr. A retreat of ice northward of the Taimyr Peninsula during the MIS 5c interval is documented by the deposition of local glaciomarine sediments that were collected over various years in several studies, but recently reviewed by Möller et al. (2019a, b). Despite clear evidence of ice retreat, the timing of this retreat has low precision, and may have occurred at any time between MIS 5d and MIS 5b.

North America: During MIS 7c and 5c, most but not all of the simulated NA ice sheet retreated back (Figure 9). The larger NA ice sheet retreated faster than the EA ice sheet with rates of 14312 ± 13821 m/yr during MIS 5d-c and 28215 ± 10747 m/yr during MIS 7d-c. The retreat of the NA ice sheets during MIS 5c is supported by some geological data. From the periphery of the glaciated region, shoreline deposits on Banks and Victoria islands support ice-free conditions at $\sim$ 100 ka (Causse and Vincent, 1989) and similarly timed ice-free conditions are suggested for some areas of Baffin Island (Briner et al., 2007) as well as Atlantic Canada (Vernal et al., 1986; Rémillard et al., 2017). Evidence from the central region of the former ice sheet also supports ice-free conditions during MIS 5c between 105 ka and 95 ka (Allard et al., 2012; Dubé-Loubert et al., 2013).

3.4 Inter-ensemble variability

Selecting ensemble members with (nearly) the same global ice volume at MIS 5d reveals that different ice sheet configurations are possible for the same global eustatic sea level. The two example ensemble members in Figure 10 have the same maximum ice volume at MIS 5d, while one member (blue) has a larger NA, EA, and Greenland ice volume but a smaller Antarctic ice sheet than the other member (red).

https://doi.org/10.5194/egusphere-2025-495
Preprint. Discussion started: 18 February 2025

Generally, ensemble members display the same behaviour in both glacial inceptions, as seen in the comparison of ice margins for 5 selected members in Figure 11. Ensemble members that display the most extensive ice during the penultimate inception (thin lines) also display a large ice sheet during the last glacial inception (thick lines).

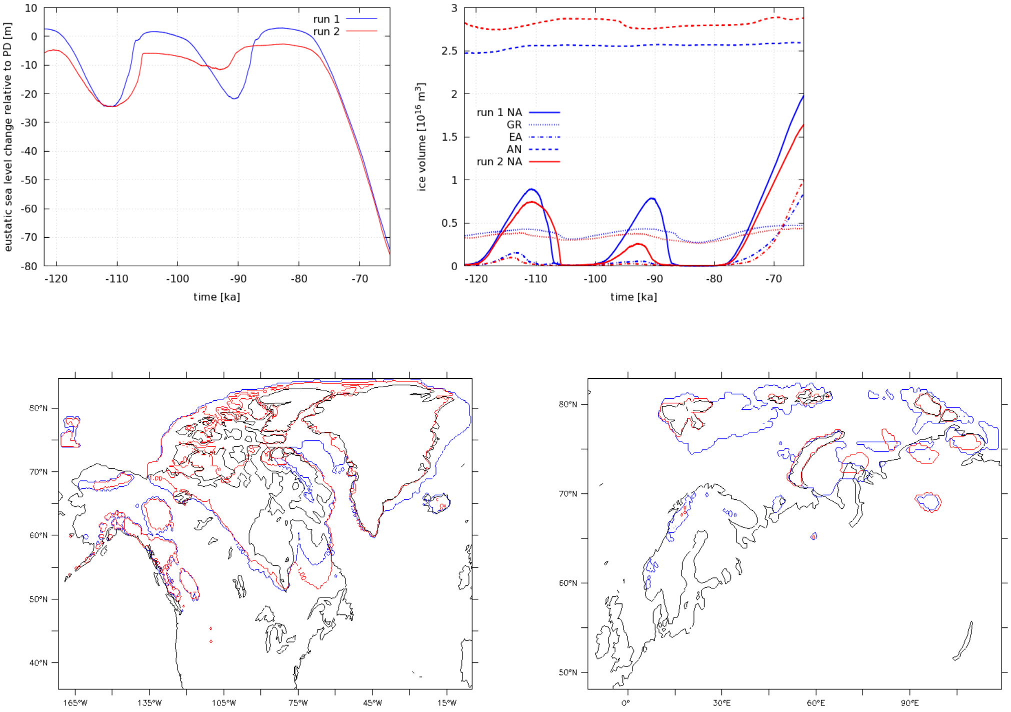

Figure 10. Two example NROY ensemble members with similar global ice volume at MIS 5d (top left) but different ice volume distribution among the ice sheets (top right) and ice sheet geometry (bottom).

4 Discussion and Conclusion

Herein, we have tested the capability of a fully coupled Earth system model, LCice, to capture the last two glacial inceptions and subsequent interstadials when only forced with orbital parameters and greenhouse gases. We have identified and analyzed an NROY subset of ensemble members that simulate sea level change within the range of proxy uncertainty for MIS 7e-7c and MIS 5e-5c. In the following, discussion of key features of the NROY ensemble is tailored to specific audiences.

4.1 Insights into ice sheet evolution

Presently, despite some recent efforts to compile geological data, little is known about the evolution of ice sheet extent through the last two glacial inceptions. One of the most extensive compilation efforts was Batchelor et al. (2019), who assembled a large

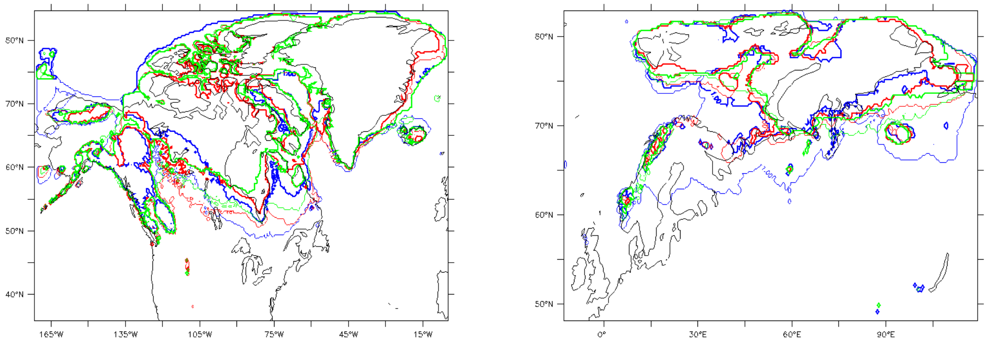

Figure 11. Ice margins of several NROY ensemble members indicated in the same colours at MIS 7d (thin line) and MIS 5d (thick line) maximum area for NA (left) and MIS 5d EA (right).

amount of numerical and geological data to give estimates on ice extent in the Northern Hemisphere through various intervals during the Quaternary. Despite their efforts, Batchelor et al. (2019) acknowledge significant unknowns and data gaps in our collective knowledge of Quaternary ice configurations. Moreover, their ice extent estimates often rely on poorly constrained model results that were never designed to probe uncertainties. In another effort, Dalton et al. (2022) used a combination of chronostratigraphic records (often rare), geomorphic data (poorly dated), estimates of global mean sea level (potentially biased in a variety of ways) and previously published ice sheet models to derive outlines of pre-LGM NA ice sheet extent. Taking into account both the work of Batchelor et al. (2019) and Dalton et al. (2022), the reconstructions for MIS 5d and c are all of “low confidence” and the onset of MIS 7 ice sheets are not investigated.

As LCIce has significant sources of unquantified uncertainty (especially on the climate side), the simulation results should not be interpreted as reconstructions. Instead, each individual simulation should be treated as a physically-self-consistent hypothesis. However, ice sheet evolution characteristics that are prevalent across the ensemble have some arguable inferential value albeit subject to the model limitations discussed in the model description above. Where model biases are large, results are more uncertain. The applied PD temperature bias correction is reduced as a function of simulated global mean sea level (relative to present) and model biases still play an unquantified role. This may especially influence results over Quebec (warm PD biases and little simulated ice) and Scandinavia (dry PD bias and little simulated ice). Furthermore, as discussed above, the limited spatial resolution of LOVECLIM will significantly affect its ability to fully capture atmospheric stationary wave changes over EA due to NA ice sheet forcing. This will in turn affect the fidelity of changes in precipitation (storm tracks) and the amplitude of the seasonal cycle, especially in Northern Russia.

4.1.1 Growth and retreat rates

Given that the simulations span intervals of ice sheet expansion (7d, 5d) and retreat (7c, 5c), the LCice ensemble can provide some physically self-consistent (though incomplete) bounds on rates of ice advance and retreat through the last glacial cycle.

Hudson Bay can transition from an ice free state to full ice cover (grounded ice) within 2000 years in the NROY ensemble (11 of 14 members glaciated Hudson Bay during MIS 7d within 2000 years). This has relevance for both empirical and numerical workers studying the dynamics of the NA ice sheet evolution and build-up toward the LGM (Dalton et al., 2018; Gauthier et al., 2019; Kleman et al., 2010). Another instance where the rate of ice growth over Hudson Bay is of interest is for the debate surrounding the potential for, and timing of, ice-free conditions during MIS 3 (Dalton et al., 2019; Hodder et al., 2023; Miller and Andrews, 2019). A major concern with the ice-free hypothesis was the feasibility of rapid ice growth over Hudson Bay (along with concerns surrounding chronology, see Dalton et al., 2019). Since LCice simulates that Hudson Bay can glaciate fully in 1000 years, it lends some support to the hypothesis that Hudson Bay may have deglaciated at some point during MIS 3. The rate of deglaciation of Hudson Bay is less enigmatic, and geological deglaciation studies have shown that ice retreated in less than 1000 years (Brouard et al., 2021; Dalton et al., 2023; Gauthier et al., 2020).

Given dating uncertainties, ice sheet advance and retreat rates can only be inferred from geological data over extended time intervals with any confidence. Given the constraint of inception and subsequent interstadial inferred sea levels, the simulations offer plausible and physically-self-consistent estimates of past advance and retreat rates. The mean NROY ensemble has a maximum NA ice sheet advance rate of 168 ± 35 m/yr during penultimate and 97 ± 35 m/yr at the southern margin during last glacial inception, while the NROY EA maximum ice sheet growth rate is 73 ± 84 m/yr for MIS 5d-c and 158 ± 45 m/yr for MIS 7d-c. Advance and retreat rates are derived from the latitude of the southernmost ice extent during growth and melt phase along a single longitude transect. The high standard deviation indicates that advance (retreat) from north to south (south to north) was by no means linear. While the over all ice area increased, the location of the southernmost ice extent can stagnate or even retreat. During the initial growth phase, snow fields can turn into ice quickly, which would lead to a fast margin advance in the model. Furthermore, the margin can "jump" large distances if advance (retreat) takes place in east-west directions rather than north-south, as it can only be evaluated along one longitude in the model. Advance rates for ice sheets are not frequently reported in the literature, so it is difficult to compare these data with other studies. The ensemble mean maximum NA retreat rate is a magnitude larger than the growth rate with over 1000 m/yr during MIS5d-c, and well over 2000 m/yr at southern margin during MIS 7d-c (larger ice sheet, faster retreat, 2). The mean NROY EA ice sheet retreat rate is over 300 m/yr during MIS 5d-c and over 900 m/yr during MIS 7d-c. These retreat rates are similar to the modern retreat of $>$ 100 m/yr seen in some areas of the Atlantic Arctic (Carr et al., 2017) and are comparable to the 50 to 80 m/yr estimate obtained for NA ice sheets by (Dalton et al., 2022).

4.1.2 Pre-LGM merging of the northern Laurentide and Cordilleran ice sheets

A characteristic of the NROY simulations is the tendency for the Laurentide and Cordilleran ice sheets to merge in their northern sectors in all but one of the simulations for MIS 7d (Figure 9). This coalescence of the Laurentide and Cordilleran ice sheets contradicts the traditional geological understanding of these ice masses. It is widely believed that they remained independent throughout the Quaternary and merged only during the LGM (Batchelor et al., 2019). Evidence in support of this assertion comes from the stratigraphic records over the Canadian Prairies. Moving westward across the Canadian Prairies, pre-glacial sediments (known as the Empress Group) are overlain only by fewer and fewer tills until they are overlain by only a single till west of Edmonton. In that area, pre-glacial tills date to 30 ka (Young et al., 1994). If one makes the big assumption that previous glacial expansions did not remove previous tills, this suggests that Laurentide ice only advanced to the Rocky Mountains once during the Quaternary, and this must have occurred after 30 ka. However, the results herein, along with the work of Evans et al. (2021) suggests that the Cordilleran and Laurentide ice sheets may have merged farther northward prior to the LGM.

What could have been the cause of the long-standing separation of southern Launretide and Cordilleran ice sheets? Herrington and Poulsen (2012), using an Atmospheric General Circulation Model, find that a glacial anticyclone established over their Laurentide ice sheet that transports warm air to the south-western ice margin and keeps the Laurentide ice sheet from merging with the Cordilleran. However, Herrington and Poulsen (2012) use steady-state simulations and lack critical ice-climate feedbacks (e.g. they use a slab ocean). Furthermore, their NA ice sheet doesn't extend south of Hudson Bay. These limitations leave unclear what the impact of such an anticyclone would be under full stadial ice extents. While a weak anticyclone develops over the Laurentide ice sheet in LCice, the strongest winds lie over the ice, and there is no transport of warm air to the south-western ice margin (Figure B13). A caveat is that LCice's atmosphere might be too coarse and simplified to fully capture this potential phenomenon.

4.1.3 Ice sheet extent and isotherm correlation

The alignment of paleo-ice sheet margins with isotherms can help inform past ice sheet extent from temperature reconstructions where there are no geological constraints. During the advance of the NA ice sheet, the simulated southern ice margin aligns with the JJA-2°C isotherm in most areas. At maximum extent, the ice margin lies between the -2 and 0°JJA isotherm. During the retreat phase, the stronger margin ice flux pushes ice margin to or beyond the 4°isotherm. Mountainous regions like the Cordilleran lie south of the aforementioned isotherms, as the isotherms are evaluated on sea level. The EA ice sheet has largely marine margins during advance and retreat phases and even during MIS 5d. For the continental margins during MIS 7d the same relationship as for the Laurentide ice sheet exists; the ice margin lies between the -2 and 0°JJA isotherms.

4.2 Implications for the sea level community

Rates of sea level change derived from proxy records have high uncertainties given the amplification of age uncertainties by the derivative operation. Given the filtering of simulations to be approximately consistent the approximate sea level record, our model derived rates of changes should have relatively high confidence. The simulated mean growth rates are 4.6 ± 1.0 mSLE/kyr for the NA ice sheet building up to MIS 7d and 3.0 ± 0.5 mSLE/kyr to MIS 5d. Net mass loss rates can be more than twice as large, with 9.7 ± 7.6 mSLE/kyr following MIS 7d and 6.8 ± 4.3 mSLE/kyr following MIS 5d. Melt and growth

https://doi.org/10.5194/egusphere-2025-495
Preprint. Discussion started: 18 February 2025

rates are smaller for the EA ice sheet (2.6 ± 0.9 mSLE/kyr and 1.3 ± 0.5 mSLE/kyr leading up to MIS 7d and 5d and 4.1 ± 5.8 mSLE/kyr and 0.8 ± 1.4 mSLE/kyr following MIS 7d and 5d respectively, see all values in Table 2).

Age control prior to the ^{14}C calibration is an outstanding challenge, necessitating, for instance, a reliance on orbitial tuning of marine records. The impact of the age uncertainties are very evident in the different timing of MIS 7d and MIS 5b between the global mean sea level reconstructions of Medina-Elizalde (2013) and Spratt and Lisiecki (2016) shown in Figure 1. Given the incorporated physics, the timing of glacial stadial maxima and interstadials in LCIce should be relatively confident for NA and at most slightly advanced for EA given atmospheric grid resolution limitations. The timing of simulated sea level high/low stands matches that of the reconstructed sea level at MIS 7d, 7c, 5d, and 5c within proxy uncertainties.

The timing of maximum ice volume lags behind the insolation minimum. A correlation exists, where larger ice sheets display a larger lag. However, we reason that this is dependent not only on the size of an ice sheet but also on the ice sheet's geometry. The smaller EA ice sheet has a higher ratio of ice margin (and therefore calving and ablation zones) to ice volume as it consists of several smaller ice sheets during the periods examined here, while the larger NA (as well as Greenland) ice sheet consists of a more contiguous ice sheet. The size of the ice sheet will also come into direct play, given the larger impact of a larger ice sheet on regional climate. This along with geographic proximity to NA also partly explains the larger lag for Greenland compared to EA.

4.3 Implications for the modeling community

The fully coupled Earth system model of intermediate complexity LCice can simulate the evolution of ice volume within proxy uncertainty for MIS 7 and MIS 5. However, it is evident that a model's capability to simulate present-day climate is insufficient to predict its performance in simulating glacial inception, as only a small fraction of ensemble members performed well for both glacial inceptions. Furthermore, capturing sea level change well in one inception does not predict the same outcome for the other. Nevertheless, an ensemble member's overall behaviour (regarding ice sheet size and geometry) is similar in both simulation periods (Figure 11). Therefore, an ensemble member that displays excessive ice growth still within the bounds in one inception might display the same behaviour slightly stronger in the other inception and miss the bounds of the accepted range. We do not see contrasting ice volume behaviour of one and the same ensemble member in the two inceptions. However, at the same simulated eustatic sea level, ensemble members can display different ice sheet configurations (Figure 10). This has high relevance for the selection of ice sheet boundary conditions for paleoclimate modeling, especially since deglacial ice sheet reconstructions are often used for pre-LGM boundary conditions by matching sea levels. Our ensemble results challenge the validity of this approach.

Simulating ice-free Alaska and Siberia during glacial inceptions remains difficult, as previous studies have shown (Willeit et al., 2023; Bahadory et al., 2021; Ganopolski et al., 2010; Bonelli et al., 2009). Compared to previous studies employing an earlier version of LCice (Bahadory and Tarasov, 2018; Bahadory et al., 2021), this current model version improves the simulation of the expected NA ice sheet geometry, at least in part due to the imposition of present-day bias corrections. However bias corrections are a bitter pill, with limited justification for modeling climate response to large changes in radiative forcing and boundary conditions. This a core challenge for all coupled paleo ice-climate modeling as even the advanced General

Circulation Models that participated in the recent CMIP6 have signficant regional present-day temperature and precipitation biases (e.g. Fan et al., 2020). It remains an open question how these biases should be addressed over glacial intervals for coupled ice and climate model at any level of computationally tractable complexity.

To build confidence in the detailed simulated evolution of coupled ice and climate, there is a need for effectively higher climate model resolution (equivalent to T42 or higher as discussed above) and complexity, which is beyond commonly available computational resources. A possible solution is the development of alternative fast climate models perhaps combining physics informed deep learning with reduced complexity climate models.

Code availability. none

Data availability. none

Video supplement. Ice sheet evolution of 14 NROY simulations for MIS 7e-7c; https://doi.org/10.5446/69809

Video supplement. Ice sheet evolution of 14 NROY simulations for MIS 5e-5c; https://doi.org/10.5446/69808

https://doi.org/10.5194/egusphere-2025-495
Preprint. Discussion started: 18 February 2025

Appendix A: Appendices to Methods

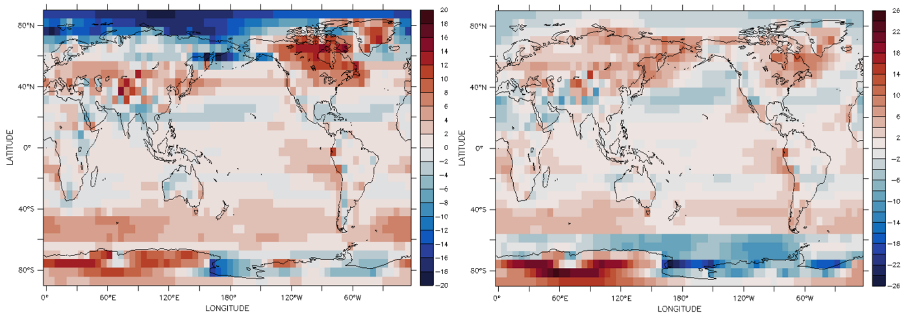

LCice − ERA5 DJF T2m

LCice − ERA5 JJA T2m

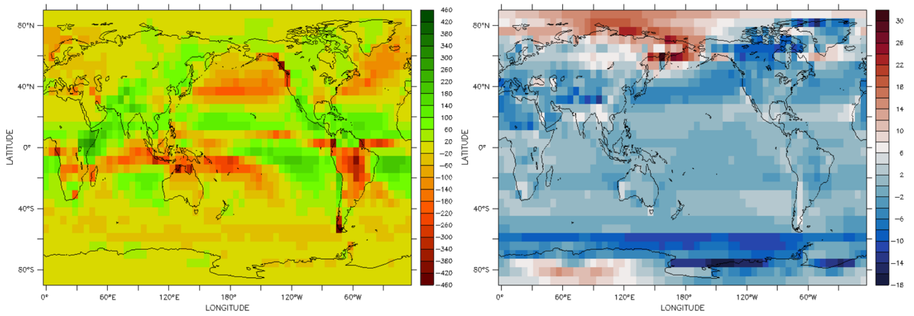

LCice − ERA5 annual average precip

LCice − ERA5 JJA − DJF

Figure A1. Sub-ensemble mean seasonal temperature (DJF top left, JJA top right), annual precipitation (bottom left), and seasonal range (JJA-DJF temperature, bottom right) biases compared to ERA 5.

https://doi.org/10.5194/egusphere-2025-495
Preprint. Discussion started: 18 February 2025

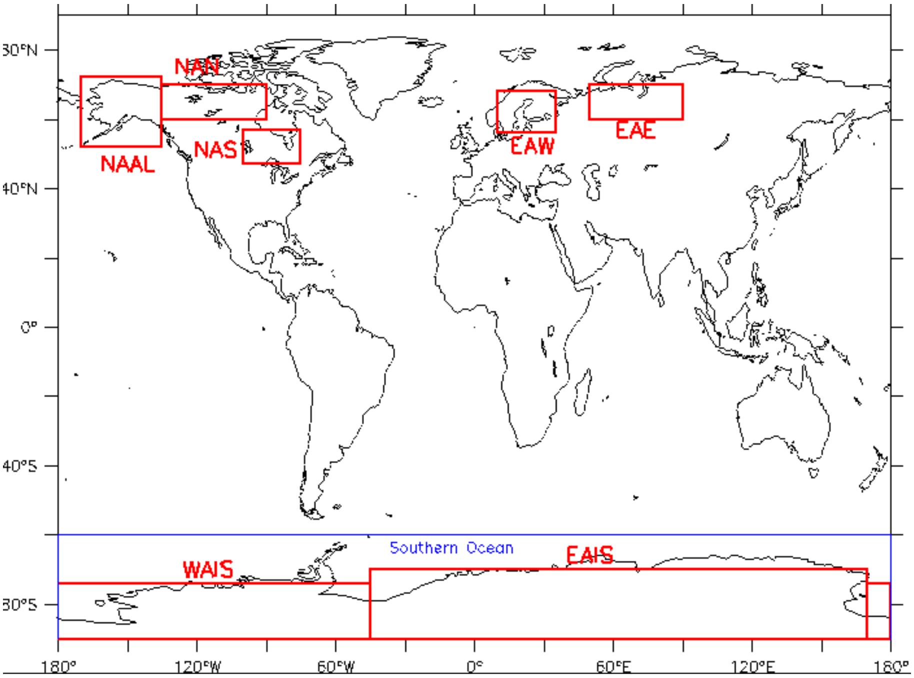

Figure A2. Regions for filtering PD simulations against reanalysis

https://doi.org/10.5194/egusphere-2025-495
Preprint. Discussion started: 18 February 2025

525 ## Appendix B: Appendices to Results

Table B1. Mean LOVECLIM parameter values and standard deviation for the full ensemble (“all members”), the sub-ensemble passing sea-level filters for MIS 5d, 5c and 4 (“pass inc”), the sub-ensemble passing sea-level filters for MIS 7d, 7c and 6e (“pass peninc”), the sub-ensemble passing all filters, and the default values

Parameter	all members	pass inc	pass peninc	pass all filters	default
ampwir	0.9 ± 0.2	0.9 ± 0.2	0.8 ± 0.2	0.9 ± 0.1	1.0
ampeqir	1.8 ± 0.4	1.8 ± 0.5	1.8 ± 0.5	2.0 ± 0.4	1.8
expir	0.34 ± 0.06	0.33 ± 0.07	0.34 ± 0.07	0.35 ± 0.04	0.40
cdrag	0.0013 ± 0.0002	0.0013 ± 0.0003	0.0013 ± 0.0003	0.0013 ± 0.0001	0.0014
evfac	0.8 ± 0.1	0.8 ± 0.2	0.8 ± 0.2	0.80 ± 0.09	1.00
cwdrag	0.0017 ± 0.0006	0.0019 ± 0.0007	0.0017 ± 0.0006	0.0018 ± 0.0004	0.0021
ahu	99193 ± 23718	99929 ± 26863	96266 ± 25322	99673 ± 21792	100000
uv10rfx	0.78 ± 0.09	0.8 ± 0.1	0.8 ± 0.1	0.78 ± 0.04	0.80
relhmax	0.8 ± 0.1	0.8 ± 0.1	0.8 ± 0.1	0.81 ± 0.04	0.83
albet	0.13 ± 0.02	0.13 ± 0.03	0.13 ± 0.03	0.14 ± 0.02	0.13
albeg	0.21 ± 0.03	0.21 ± 0.03	0.21 ± 0.03	0.21 ± 0.01	0.20
albed	0.33 ± 0.05	0.32 ± 0.06	0.34 ± 0.07	0.33 ± 0.04	0.33
alphd	0.7 ± 0.1	0.7 ± 0.1	0.7 ± 0.1	0.72 ± 0.05	0.72
alphdi	0.57 ± 0.07	0.57 ± 0.10	0.57 ± 0.09	0.58 ± 0.03	0.62
alphs	0.50 ± 0.08	0.49 ± 0.10	0.48 ± 0.09	0.48 ± 0.05	0.53
albice	0.38 ± 0.07	0.37 ± 0.08	0.37 ± 0.08	0.37 ± 0.05	0.44
GHG	2.1 ± 0.4	2.2 ± 0.4	2.1 ± 0.4	2.2 ± 0.2	1.0

Table B2. Parameter short names and description

ampwir	amplification factor longwave radiation
ampeqir	amplification factor longwave radiation equatorial region
expir	longwave radiation exponent to moisture
cdrag	coeff. in sensible and latent air-sea heat flux
evfac	max. evaporation factor over land
cwdrag	wind stress coeff.
ahu	ocean horizontal viscosity
uv10rfx	800 hPa wind speed reduction to 10 m
relhmax	precipitation threshold
albet	tree albedo
albeg	grass abledo
albed	dessert albedo
alphd	albedo of snow
alphdi	albedo of ice
alphs	albedo of melting snow

https://doi.org/10.5194/egusphere-2025-495
Preprint. Discussion started: 18 February 2025

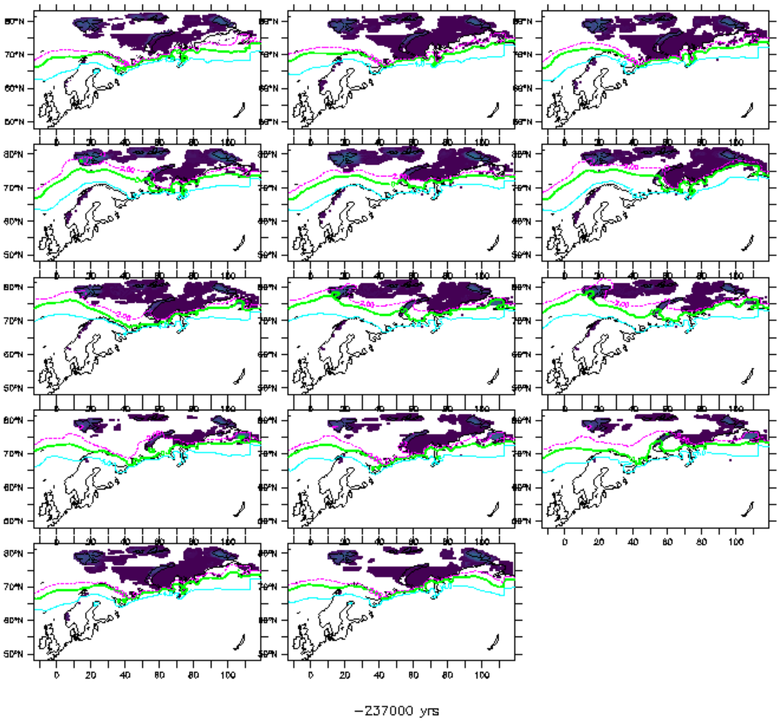

Figure B1. Ice height and +4°(light blue), 0°(green), and -2°(pink) isotherms during Eurasian ice advance phase towards MIS 7d

https://doi.org/10.5194/egusphere-2025-495
Preprint. Discussion started: 18 February 2025

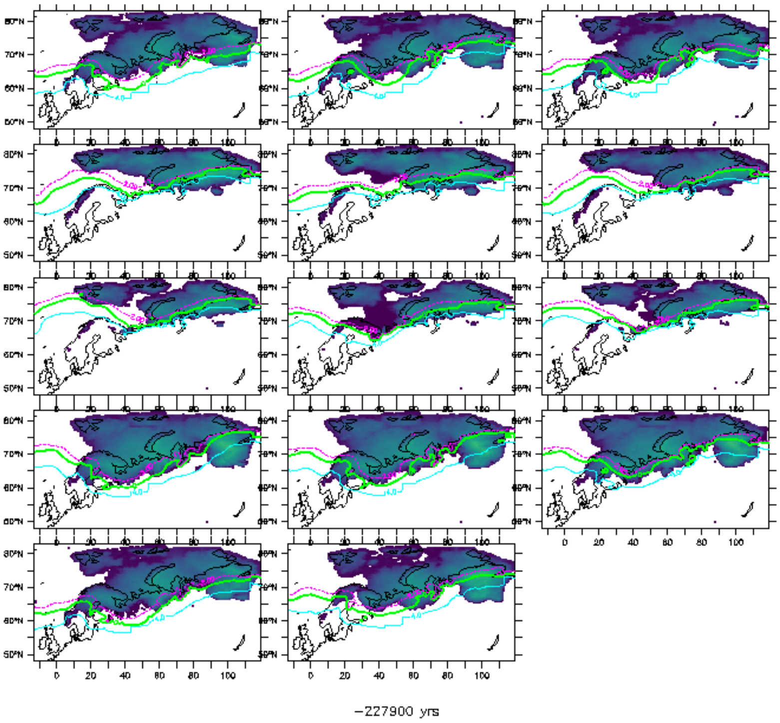

Figure B2. Ice height and +4°(light blue), 0°(green), and -2°(pink) isotherms during Eurasian max. ice extent at MIS 7d

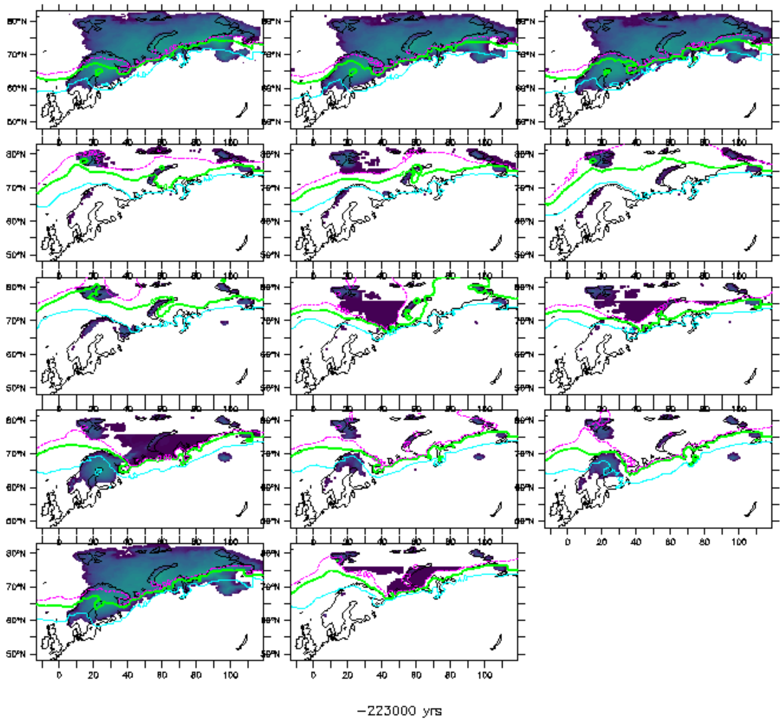

Figure B3. Ice height and +4°(light blue), 0°(green), and -2°(pink) isotherms during Eurasian ice retreat phase after MIS 7d

https://doi.org/10.5194/egusphere-2025-495
Preprint. Discussion started: 18 February 2025

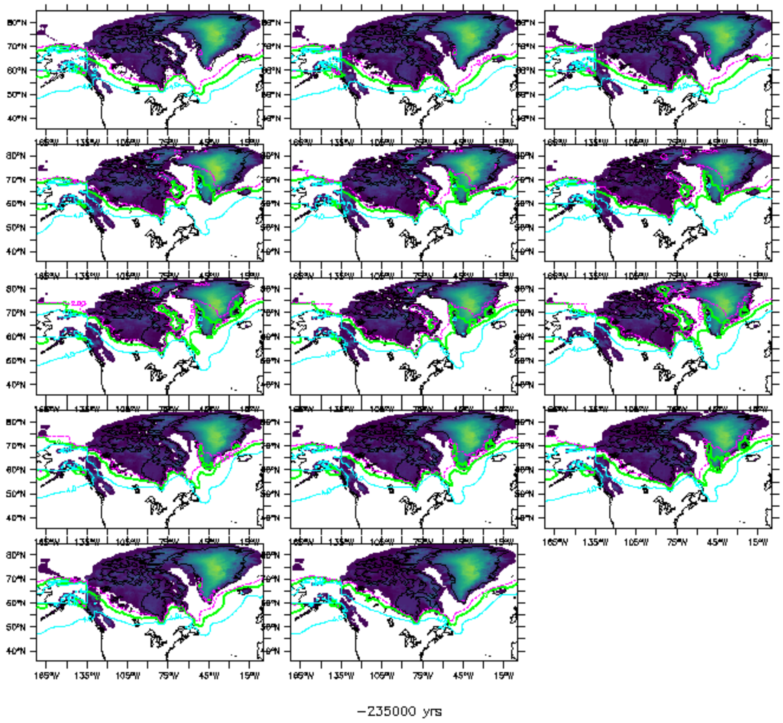

Figure B4. Ice height and +4°(light blue), 0°(green), and -2°(pink) isotherms during North American ice advance phase towards MIS 7d

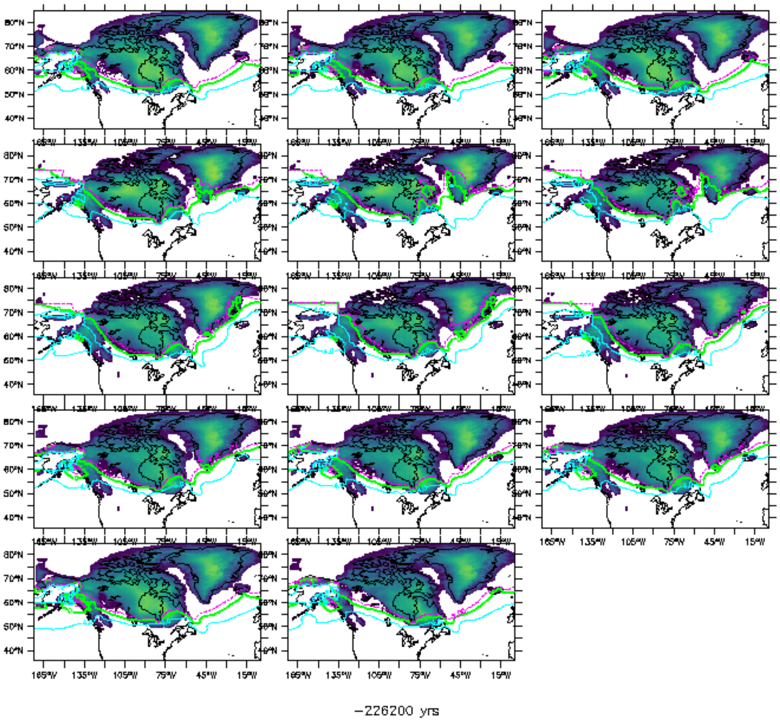

Figure B5. Ice height and +4°(light blue), 0°(green), and -2°(pink) isotherms during North American max. ice extent at MIS 7d

https://doi.org/10.5194/egusphere-2025-495
Preprint. Discussion started: 18 February 2025

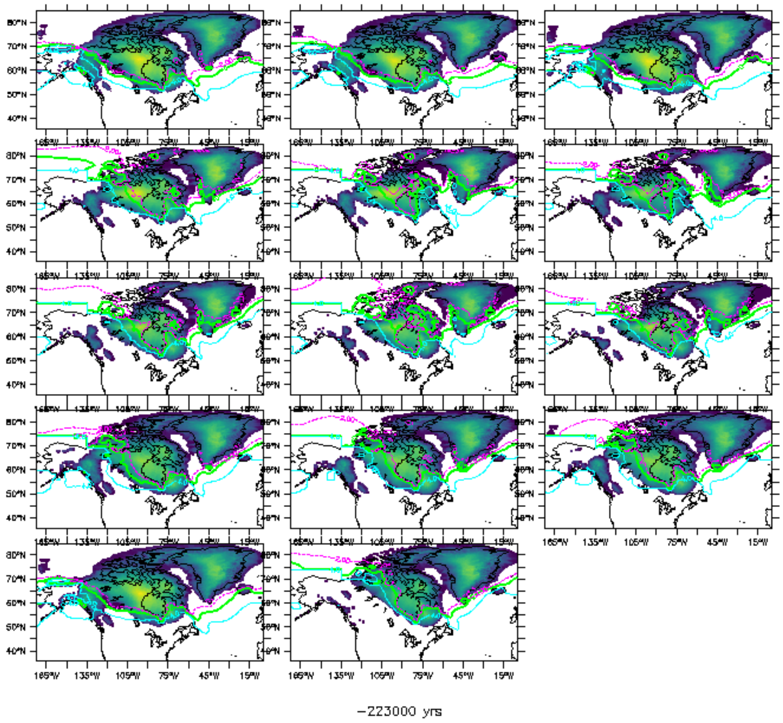

Figure B6. Ice height and +4°(light blue), 0°(green), and -2°(pink) isotherms during North American ice retreat phase after MIS 7d

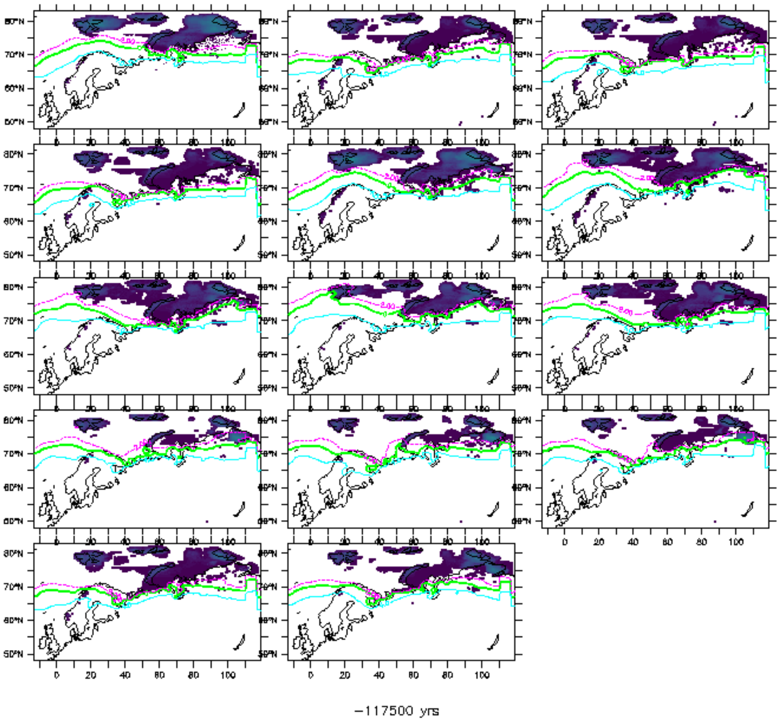

Figure B7. Ice height and +4°(light blue), 0°(green), and -2°(pink) isotherms during Eurasian ice advance phase towards MIS 5d

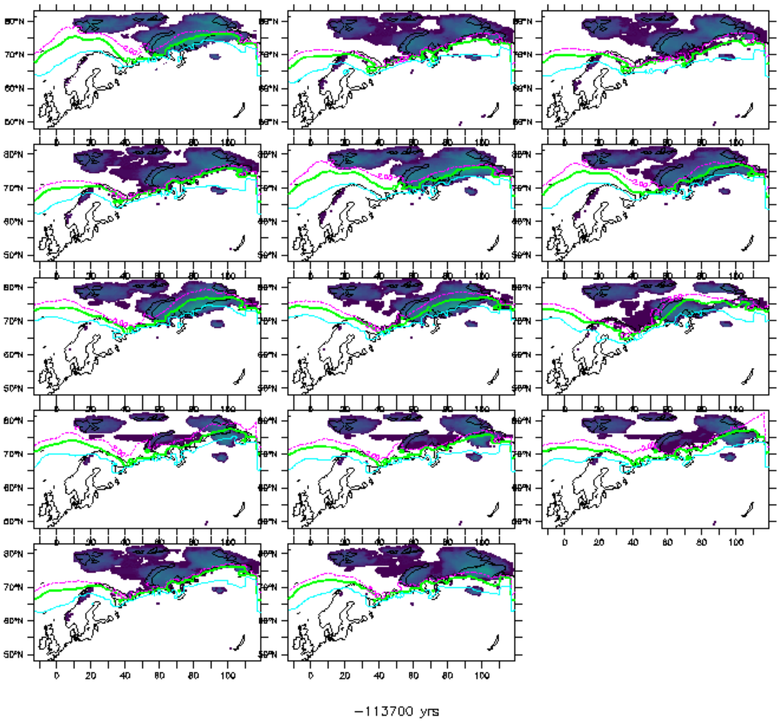

Figure B8. Ice height and +4°(light blue), 0°(green), and -2°(pink) isotherms during Eurasian max. ice extent at MIS 5d

https://doi.org/10.5194/egusphere-2025-495
Preprint. Discussion started: 18 February 2025

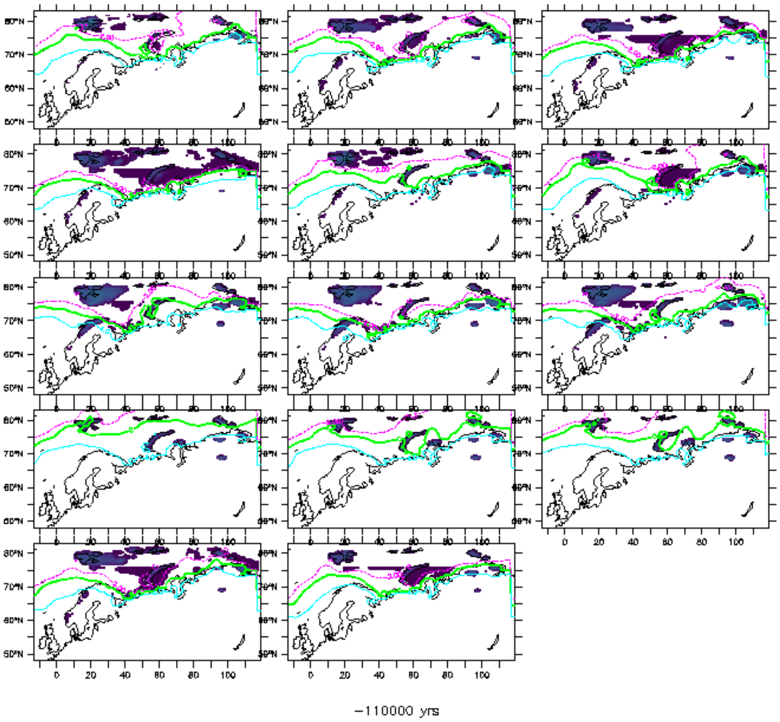

Figure B9. Ice height and +4°(light blue), 0°(green), and -2°(pink) isotherms during Eurasian ice retreat phase after MIS 5d

https://doi.org/10.5194/egusphere-2025-495
Preprint. Discussion started: 18 February 2025

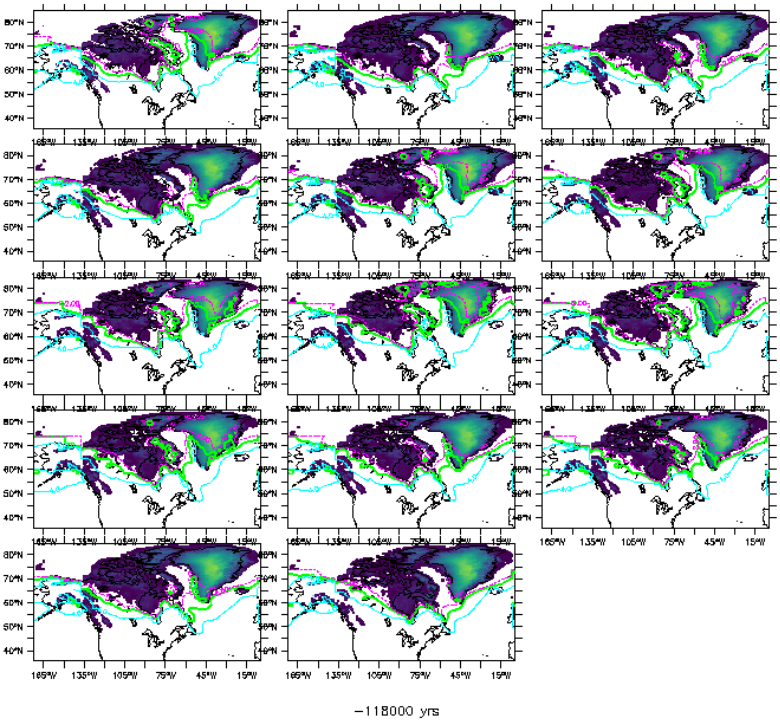

Figure B10. Ice height and +4°(light blue), 0°(green), and -2°(pink) isotherms during North American ice advance phase towards MIS 5d

https://doi.org/10.5194/egusphere-2025-495
Preprint. Discussion started: 18 February 2025

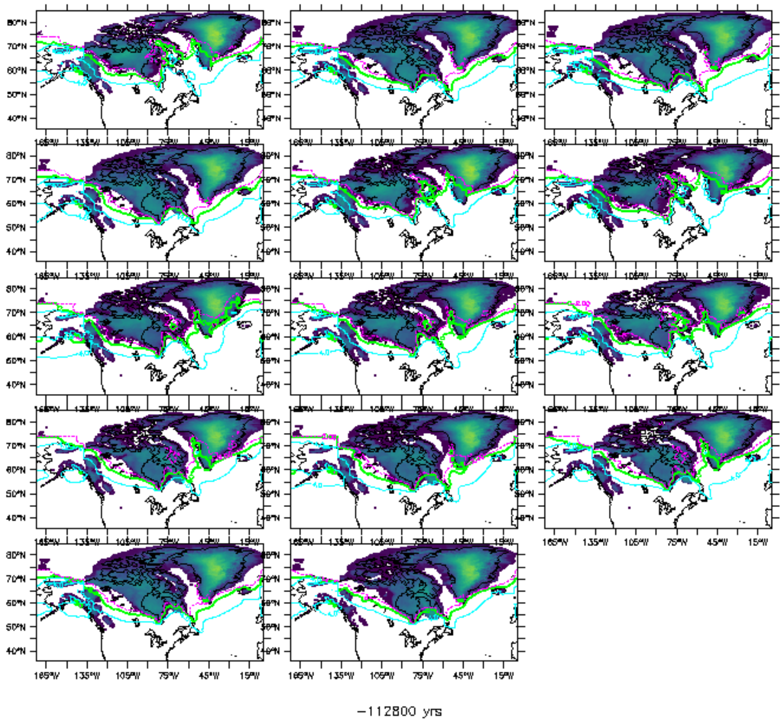

Figure B11. Ice height and +4°(light blue), 0°(green), and -2°(pink) isotherms during North American max. ice extent at MIS 5d

https://doi.org/10.5194/egusphere-2025-495
Preprint. Discussion started: 18 February 2025

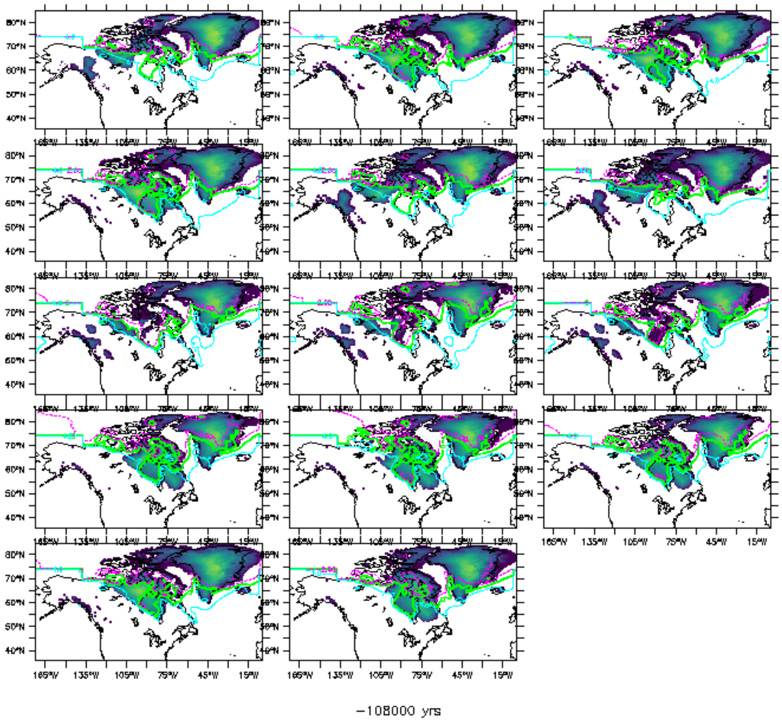

Figure B12. Ice height and +4°(light blue), 0°(green), and -2°(pink) isotherms during North American ice retreat phase after MIS 5d

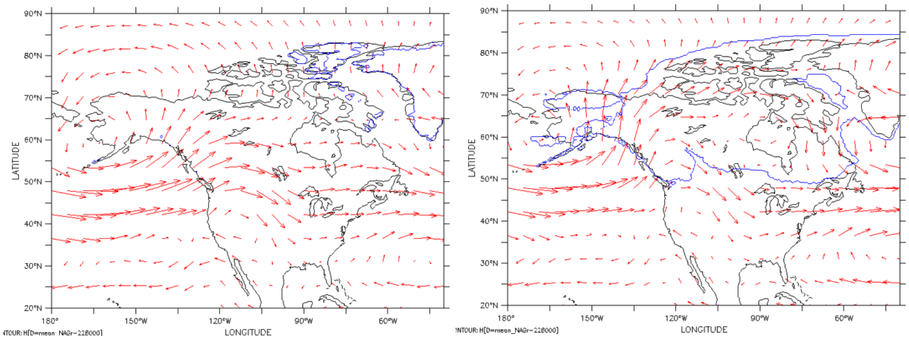

Figure B13. Sub-ensemble mean 800 hPa January wind at simulation start (interglacial conditions, MIS 7e, left) and at MIS 7d (right)

Author contributions. The authors confirm contribution to the paper as follows: study conception and design: LT, MSG; experiments: MSG; model developpment: LT, MSG; analysis and interpretation of results: MSG, LT, ASD; draft manuscript preparation: MSG, LT, ASD. All authors reviewed the results and approved the final version of the manuscript.

Competing interests. One author (Lev Tarasov) is a member of the editorial board of "Climate of the Past". The other authors declare that they have no conflict of interest.

Acknowledgements. This research has been supported by an NSERC Discovery grant (grant no. RGPIN-2018-06658), the Canadian Foundation for Innovation, and the German Federal Ministry of Education and Research (BMBF) as a Research for Sustainability initiative (FONA) through the PalMod project. This reasearch has furthermore benefited from the ArcTrain (Processes and impacts of climate change in the North Atlantic Ocean and the Canadian Arctic) training program.

References

Allard, G., Roy, M., Ghaleb, B., Richard, P. J., Larouche, A. C., Veillette, J. J., and Parent, M.: Constraining the age of the last interglacial–glacial transition in the Hudson Bay lowlands (Canada) using U–Th dating of buried wood, Quaternary Geochronology, 7, 37–47, https://doi.org/10.1016/J.QUAGEO.2011.09.004, 2012.

Andriashek, L. D. and Barendregt, R. W.: Evidence for Early Pleistocene glaciation from borecore stratigraphy in north-central Alberta, Canada, Canadian Journal of Earth Sciences, 54, 445–460, https://doi.org/10.1139/cjes-2016-0175, 2017.

Astakhov, V. and Semionova, L.: The penultimate interglaciation of northern Russia, Quaternary International, 605-606, 142–154, https://doi.org/10.1016/j.quaint.2020.12.034, 2021.

Astakhov, V., Shkatova, V., Zastrozhnov, A., and Chuyko, M.: Glaciomorphological Map of the Russian Federation, Quaternary International, 420, 4–14, https://doi.org/10.1016/J.QUAINT.2015.09.024, 2016.

Bahadory, T. and Tarasov, L.: LCice 1.0-a generalized Ice Sheet System Model coupler for LOVECLIM version 1.3: Description, sensitivities, and validation with the Glacial Systems Model (GSM version D2017.aug17), Geoscientific Model Development, 11, 3883–3902, https://doi.org/10.5194/gmd-11-3883-2018, 2018.

Bahadory, T., Tarasov, L., and Andres, H.: Last glacial inception trajectories for the Northern Hemisphere from coupled ice and climate modelling, Climate of the Past, 17, 397–418, https://doi.org/10.5194/cp-17-397-2021, 2021.

Batchelor, C. L., Margold, M., Krapp, M., Murton, D. K., Dalton, A. S., Gibbard, P. L., Stokes, C. R., Murton, J. B., and Manica, A.: The configuration of Northern Hemisphere ice sheets through the Quaternary, Nature Communications, 10, 1–10, https://doi.org/10.1038/s41467-019-11601-2, 2019.

Bates, S. L., Siddall, M., and Waelbroeck, C.: Hydrographic variations in deep ocean temperature over the mid-Pleistocene transition, Quaternary Science Reviews, 88, 147–158, https://doi.org/10.1016/j.quascirev.2014.01.020, 2014.

Bereiter, B., Eggleston, S., Schmitt, J., Nehrbass-Ahles, C., Stocker, T. F., Fischer, H., Kipfstuhl, S., and Chappellaz, J.: Revision of the EPICA Dome C CO2 record from 800 to 600-kyr before present, Geophysical Research Letters, 42, 542–549, https://doi.org/10.1002/2014GL061957, 2015.

Bonelli, S., Charbit, S., Kageyama, M., Ramstein, G., Dumas, C., and Quiquet, A.: Investigating the evolution of major Northern Hemisphere ice sheets during the last glacial-interglacial cycle, Climate of the Past, pp. 329–345, https://doi.org/10.5194/cp-5-329-2009, 2009.

Born, A., Kageyama, M., and Nisancioglu, K. H.: Warm Nordic Seas delayed glacial inception in Scandinavia, Climate of the Past, 6, 817–826, https://doi.org/10.5194/cp-6-817-2010, 2010.

Briner, J. P., Axford, Y., Forman, S. L., Miller, G. H., and Wolfe, A. P.: Multiple generations of interglacial lake sediment preserved beneath the Laurentide Ice Sheet, Geology, 35, 887–890, https://doi.org/10.1130/G23812A.1, 2007.

Brouard, E., Roy, M., Godbout, P. M., and Veillette, J. J.: A framework for the timing of the final meltwater outbursts from glacial Lake Agassiz-Ojibway, Quaternary Science Reviews, 274, 107 269, https://doi.org/10.1016/J.QUASCIREV.2021.107269, 2021.

Calov, R., Ganopolski, A., Claussen, M., Petoukhov, V., and Greve, R.: Transient simulation of the last glacial inception. Part I: Glacial inception as a bifurcation in the climate system, Climate Dynamics, 24, 545–561, https://doi.org/10.1007/s00382-005-0007-6, 2005.

Campbell, J. E., Little, E. C., Utting, D., and McMartin, I.: Surficial geology, Nanuraqtalik Lake, Nunavut; Geological Survey of Canada, Canadian Geoscience Map 60, https://doi.org/10.4095/292009, 2013.

Carr, J. R., Stokes, C. R., and Vieli, A.: Threefold increase in marine-terminating outlet glacier retreat rates across the Atlantic Arctic: 1992–2010, Annals of Glaciology, 58, 72–91, https://doi.org/10.1017/aog.2017.3, 2017.

Causse, C. and Vincent, J. S.: Th–U disequilibrium dating of Middle and Late Pleistocene wood and shells from Banks and Victoria islands, Arctic Canada, Canadian Journal of Earth Sciences, 26, 2718–2723, https://doi.org/10.1139/e89-231, 1989.

Cheng, H., Springer, G. S., Sinha, A., Hardt, B. F., Yi, L., Li, H., Tian, Y., Li, X., Rowe, H. D., Kathayat, G., Ning, Y., and Edwards, R. L.: Eastern North American climate in phase with fall insolation throughout the last three glacial-interglacial cycles, Earth and Planetary Science Letters, 522, 125–134, https://doi.org/10.1016/J.EPSL.2019.06.029, 2019.

Choudhury, D., Timmermann, A., Schloesser, F., Heinemann, M., and Pollard, D.: Simulating Marine Isotope Stage 7 with a coupled climate-ice sheet model, Climate of the Past, 16, 2183–2201, https://doi.org/10.5194/cp-16-2183-2020, 2020.

Colleoni, F., Masina, S., Cherchi, A., and Iovino, D.: Impact of orbital parameters and greenhouse gas on the climate of MIS 7 and MIS 5 glacial inceptions, Journal of Climate, 27, 8918–8933, https://doi.org/10.1175/JCLI-D-13-00754.1, 2014.

Copernicus, C. C. S.: ORAS5 global ocean reanalysis monthly data from 1958 to present, Climate Data Store, 2021.

Dalton, A. S., Finkelstein, S. A., Barnett, P. J., Väliranta, M., and Forman, S. L.: Late Pleistocene chronology, palaeoecology and stratigraphy at a suite of sites along the Albany River, Hudson Bay Lowlands, Canada, Palaeogeography, Palaeoclimatology, Palaeoecology, 492, 50–63, https://doi.org/10.1016/J.PALAEO.2017.12.011, 2018.

Dalton, A. S., Finkelstein, S. A., Forman, S. L., Barnett, P. J., Pico, T., and Mitrovica, J. X.: Was the Laurentide Ice Sheet significantly reduced during Marine Isotope Stage 3?, Geology, 47, 111–114, https://doi.org/10.1130/G45335.1, 2019.

Dalton, A. S., Stokes, C. R., and Batchelor, C. L.: Evolution of the Laurentide and Innuitian ice sheets prior to the Last Glacial Maximum (115 ka to 25 ka), Earth-Science Reviews, 224, 103 875, https://doi.org/10.1016/j.earscirev.2021.103875, 2022.

Dalton, A. S., Dulfer, H. E., Margold, M., Heyman, J., Clague, J. J., Froese, D. G., Gauthier, M. S., Hughes, A. L., Jennings, C. E., Norris, S. L., and Stoker, B. J.: Deglaciation of the north American ice sheet complex in calendar years based on a comprehensive database of chronological data: NADI-1, Quaternary Science Reviews, 321, 108 345, https://doi.org/10.1016/J.QUASCIREV.2023.108345, 2023.

Dubé-Loubert, H., Roy, M., Allard, G., Lamothe, M., and Veillette, J. J.: Glacial and nonglacial events in the eastern James Bay lowlands, Canada, Canadian Journal of Earth Sciences, 50, 379–396, https://doi.org/10.1139/cjes-2012-0065, 2013.

Dyke, A. S.: An outline of North American deglaciation with emphasis on central and northern Canada, in: Quaternary Glaciations-Extent and Chronology, Part II, edited by Ehlers, J. and Gibbard, P. L., vol. 2b, pp. 373–424, Elsevier, 2004.

Evans, D. J., Smith, I. R., Gosse, J. C., and Galloway, J. M.: Glacial landforms and sediments (landsystem) of the Smoking Hills area, Northwest Territories, Canada: Implications for regional Pliocene – Pleistocene Laurentide Ice Sheet dynamics, Quaternary Science Reviews, 262, 106 958, https://doi.org/10.1016/J.QUASCIREV.2021.106958, 2021.

Fan, X., Duan, Q., Shen, C., Wu, Y., and Xing, C.: Global surface air temperatures in CMIP6: Historical performance and future changes, Environmental Research Letters, 15, https://doi.org/10.1088/1748-9326/abb051, 2020.

Gallée, H., Yperselb, J. P. V., Fichefet, T., Marsiat, I., Tricot, C., and Berger, A.: Simulation of the last glacial cycle by a coupled, sectorially averaged climate-ice sheet model: 2. Response to insolation and CO 2 variations, Journal of Geophysical Research, 7, 7(D14), 15 713–15 740., https://doi.org/10.1029/92JD01256, problems: not enough ice (southern extent), needed to apply an ageing snow parameter to NH to get deglaciation. That same aging snow parameter would have made AN melt., 1992.

Ganopolski, A., Calov, R., and Claussen, M.: Simulation of the last glacial cycle with a coupled climate ice-sheet model of intermediate complexity, Climate of the Past, pp. 229–244, 2010.

Gauthier, M. S., Hodder, T. J., Ross, M., Kelley, S. E., Rochester, A., and McCausland, P.: The subglacial mosaic of the Laurentide Ice Sheet; a study of the interior region of southwestern Hudson Bay, Quaternary Science Reviews, 214, 1–27, https://doi.org/10.1016/J.QUASCIREV.2019.04.015, 2019.

Gauthier, M. S., Kelley, S. E., and Hodder, T. J.: Lake Agassiz drainage bracketed Holocene Hudson Bay Ice Saddle collapse, Earth and Planetary Science Letters, 544, 116 372, https://doi.org/10.1016/J.EPSL.2020.116372, 2020.

Goosse, H., Brovkin, V., Fichefet, T., Haarsma, R., Huybrechts, P., Jongma, J., Mouchet, A., Selten, F., Barriat, P. Y., Campin, J. M., Deleersnijder, E., Driesschaert, E., Goelzer, H., Janssens, I., Loutre, M. F., Maqueda, M. A. M., Opsteegh, T., Mathieu, P. P., Munhoven, G., Pettersson, E. J., Renssen, H., Roche, D. M., Schaeffer, M., Tartinville, B., Timmermann, A., and Weber, S. L.: Description of the Earth system model of intermediate complexity LOVECLIM version 1.2, Geoscientific Model Development, 3, 603–633, https://doi.org/10.5194/gmd-3-603-2010, 2010.

Grant, K. M., Rohling, E. J., Ramsey, C. B., Cheng, H., Edwards, R. L., Florindo, F., Heslop, D., Marra, F., Roberts, A. P., Tamisiea, M. E., and Williams, F.: Sea-level variability over five glacial cycles, Nature Communications, 5, https://doi.org/10.1038/ncomms6076, 2014.

Herrington, A. R. and Poulsen, C. J.: Terminating the last interglacial: The role of ice sheet-climate feedbacks in a GCM asynchronously coupled to an ice sheet model, Journal of Climate, 25, 1871–1882, https://doi.org/10.1175/JCLI-D-11-00218.1, 2012.

Hersbach, H., Bell, B., Berrisford, P., Hirahara, S., Horányi, A., Muñoz-Sabater, J., Nicolas, J., Peubey, C., Radu, R., Schepers, D., Simmons, A., Soci, C., Abdalla, S., Abellan, X., Balsamo, G., Bechtold, P., Biavati, G., Bidlot, J., Bonavita, M., Chiara, G. D., Dahlgren, P., Dee, D., Diamantakis, M., Dragani, R., Flemming, J., Forbes, R., Fuentes, M., Geer, A., Haimberger, L., Healy, S., Hogan, R. J., Hólm, E., Janisková, M., Keeley, S., Laloyaux, P., Lopez, P., Lupu, C., Radnoti, G., Rosnay, P. D., Rozum, I., Vamborg, F., Villaume, S., and Thépaut, J.-N.: The ERA5 global reanalysis, Q J R Meteorol Soc, 146, 1999–2049, https://doi.org/10.1002/qj.3803, 2020.

Hodder, T. J., Gauthier, M. S., Ross, M., and Lian, O. B.: Was there a nonglacial episode in the western Hudson Bay Lowland during Marine Isotope Stage 3?, Quaternary Research (United States), pp. 148–161, https://doi.org/10.1017/qua.2023.35, 2023.

Hughes, A. L., Gyllencreutz, R., Øystein S. Lohne, Mangerud, J., and Svendsen, J. I.: The last Eurasian ice sheets - a chronological database and time-slice reconstruction, DATED-1, Boreas, 45, 1–45, https://doi.org/10.1111/bor.12142, 2016.

Ives, J.: Glaciation of the Torngat Mountains, Northern Labrador, Arctic, 10, 66, https://doi.org/10.14430/arctic3755, 1957.

Kaufman, D. S., Young, N. E., Briner, J. P., and Manley, W. F.: Alaska Paleo-Glacier Atlas (Version 2), Quaternary Glaciations Extent and Chronology, Part IV: A Closer Look, 15, 427–445, 2011.

Kauman, D. S. and Manley, W. F.: Pleistocene Maximum and Late Wisconsinan glacier extents across Alaska, U.S.A., Developments in Quaternary Science, 2, 9–27, https://doi.org/10.1016/S1571-0866(04)80182-9, 2004.

Khodri, M., Leclalnche, Y., Ramstein, G., Braconnot, P., Marti, O., and Cortijo, E.: Simulating the amplification of orbital forcing by ocean feedbacks in the last glaciation, Nature, 410, 570–574, https://doi.org/10.1038/35069044, 2001.

Kleman, J., Jansson, K., Angelis, H. D., Stroeven, A. P., Hättestrand, C., Alm, G., and Glasser, N.: North American Ice Sheet build-up during the last glacial cycle, 115–21 kyr, Quaternary Science Reviews, 29, 2036–2051, https://doi.org/10.1016/J.QUASCIREV.2010.04.021, 2010.

Koerner, R. M.: Instantaneous glacierization, the rate of albedo change, and feedback effects at the beginning of an ice age, Quaternary Research, 13, 153–159, https://doi.org/10.1016/0033-5894(80)90025-3, 1980.

Laskar, J., Robutel, P., Joutel, F., Gastineau, M., Correia, A. C., and Levrard, B.: A long-term numerical solution for the insolation quantities of the Earth, Astronomy and Astrophysics, 428, 261–285, https://doi.org/10.1051/0004-6361:20041335, 2004.

Lisiecki, L. E. and Raymo, M. E.: A Pliocene-Pleistocene stack of 57 globally distributed benthic δ 18O records, Paleoceanography, 20, 1–17, https://doi.org/10.1029/2004PA001071, 2005.

Lofverstrom, M. and Liakka, J.: The influence of atmospheric grid resolution in a climate model-forced ice sheet simulation, Cryosphere, 12, 1499–1510, https://doi.org/10.5194/TC-12-1499-2018, 2018.

McMartin, I., Godbout, P. M., Campbell, J. E., Tremblay, T., and Behnia, P.: A new map of glacigenic features and glacial landsystems in central mainland Nunavut, Canada, Boreas, 50, 51–75, https://doi.org/10.1111/bor.12479, 2021.

McMartin, I., Campbell, J., Godbout, P.-M., Behnia, P., Tremblay, T., and Normandeau, P.: High-resolution mapping of glacial landscapes in the north-central portion of the Laurentide Ice Sheet in Nunavut and Northwest Territories, pp. 145–165, https://doi.org/10.4095/331423, 2023.

Medina-Elizalde, M.: A global compilation of coral sea-level benchmarks: Implications and new challenges, Earth and Planetary Science Letters, 362, 310–318, https://doi.org/10.1016/j.epsl.2012.12.001, 2013.

Miller, G. H. and Andrews, J. T.: Hudson Bay was not deglaciated during MIS-3, Quaternary Science Reviews, 225, 105 944, https://doi.org/10.1016/j.quascirev.2019.105944, 2019.

Möller, P., Fedorov, G., Pavlov, M., Seidenkrantz, M. S., and Sparrenbom, C.: Glacial and palaeoenvironmental history of the Cape Chelyuskin area, Arctic Russia, Polar Research, 27, 222–248, https://doi.org/10.1111/j.1751-8369.2008.00066.x, 2008.

Möller, P., Alexanderson, H., Funder, S., and Hjort, C.: The Taimyr Peninsula and the Severnaya Zemlya archipelago, Arctic Russia: a synthesis of glacial history and palaeo-environmental change during the Last Glacial cycle (MIS 5e–2), Quaternary Science Reviews, 107, 149–181, https://doi.org/10.1016/J.QUASCIREV.2014.10.018, 2015.

Möller, P., Ívar Örn Benediktsson, Anjar, J., Bennike, O., Bernhardson, M., Funder, S., Håkansson, L. M., Lemdahl, G., Licciardi, J. M., Murray, A. S., and Seidenkrantz, M. S.: Glacial history and palaeo-environmental change of southern Taimyr Peninsula, Arctic Russia, during the Middle and Late Pleistocene, Earth-Science Reviews, 196, 102 832, https://doi.org/10.1016/J.EARSCIREV.2019.04.004, 2019a.

Möller, P., Ívar Örn Benediktsson, Anjar, J., Bennike, O., Bernhardson, M., Funder, S., Håkansson, L. M., Lemdahl, G., Licciardi, J. M., Murray, A. S., and Seidenkrantz, M. S.: Data set on sedimentology, palaeoecology and chronology of Middle to Late Pleistocene deposits on the Taimyr Peninsula, Arctic Russia, Data in Brief, 25, 104 267, https://doi.org/10.1016/J.DIB.2019.104267, 2019b.

Otieno, F. O. and Bromwich, D. H.: Contribution of atmospheric circulation to inception of the Laurentide Ice Sheet at 116 kyr BP, Journal of Climate, 22, 39–57, https://doi.org/10.1175/2008JCLI2211.1, 2009.

Peltier, W. R. and Marshall, S.: Coupled energy-balance/ice-sheet model simulations of the glacial cycle: A possible connection between terminations and terrigenous dust, Journal of Geophysical Research, 100, 14 269, https://doi.org/10.1029/95JD00015, 1995.

Rémillard, A. M., St-Onge, G., Bernatchez, P., Hétu, B., Buylaert, J. P., Murray, A. S., and Lajeunesse, P.: Relative sea-level changes and glacio-isostatic adjustment on the Magdalen Islands archipelago (Atlantic Canada) from MIS 5 to the late Holocene, Quaternary Science Reviews, 171, 216–233, https://doi.org/10.1016/J.QUASCIREV.2017.07.015, 2017.

Spratt, R. M. and Lisiecki, L. E.: A Late Pleistocene sea level stack, Climate of the Past, 12, 1079–1092, https://doi.org/10.5194/cp-12-1079-2016, 2016.

Svendsen, J. I., Alexanderson, H., Astakhov, V. I., Demidov, I., Dowdeswell, J. A., Funder, S., Gataullin, V., Henriksen, M., Hjort, C., Houmark-Nielsen, M., Hubberten, H. W., Ólafur Ingólfsson, Jakobsson, M., Kjær, K. H., Larsen, E., Lokrantz, H., Lunkka, J. P., Lyså, A., Mangerud, J., Matiouchkov, A., Murray, A., Möller, P., Niessen, F., Nikolskaya, O., Polyak, L., Saarnisto, M., Siegert, C., Siegert, M. J., Spielhagen, R. F., and Stein, R.: Late Quaternary ice sheet history of northern Eurasia, Quaternary Science Reviews, 23, 1229–1271, https://doi.org/10.1016/j.quascirev.2003.12.008, 2004.

Tarasov, L. and Peltier, W. R.: Terminating the 100 kyr ice age cycle, Journal of Geophysical Research: Atmospheres, 102, 21 665–21 693, https://doi.org/10.1029/97JD01766, 1997.

Vernal, A. D., Causse, C., Hillaire-Marcel, C., Mott, R. J., and Occhietti, S.: Palynostratigraphy and Th/U ages of upper Pleistocene interglacial and interstadial deposits on Cape Breton Island, eastern Canada., Geology, 14, 554–557, https://doi.org/10.1130/0091-7613(1986)14<554:PATAOU>2.0.CO;2, 1986.

Vettoretti, G. and Peltier, W. R.: Post-Eemian glacial inception. Part I: The impact of summer seasonal temperature bias, Journal of Climate, 16, 889–911, https://doi.org/10.1175/1520-0442(2003)016<0889:PEGIPI>2.0.CO;2, 2003.

Willeit, M., Ganopolski, A., Robinson, A., and Edwards, N. R.: The Earth system model CLIMBER-X v1.0-Part 1: Climate model description and validation, Geoscientific Model Development, 15, 5905–5948, https://doi.org/10.5194/gmd-15-5905-2022, 2022.

Willeit, M., Calov, R., Talento, S., Greve, R., Bernales, J., Klemann, V., Bagge, M., and Ganopolski, A.: Glacial inception through rapid ice area increase driven by albedo and vegetation feedbacks, EGUsphere [preprint], pp. 1–41, 2023.

Winograd, I. J., Coplen, T. B., Landwehr, J. M., Riggs, A. C., Ludwig, K. R., Szabo, B. J., Kolesar, P. T., and Revesz, K. M.: Continuous 500,000-Year Climate Record from Vein Calcite in Devils Hole, Nevada, Science, 258, 255–260, https://doi.org/10.1126/science.258.5080.255, 1992.

Yoshimori, M., Reader, M., Weaver, A., and McFarlane, N.: On the causes of glacial inception at 116 kaBP, Climate Dynamics, 18, 383–402, https://doi.org/10.1007/s00382-001-0186-8, 2002.

Young, R. R., Burns, J. A., Smith, D. G., Arnold, L. D., and Rains, R. B.: A single, late Wisconsin, Laurentide Glaciation, Edmonton area and southwestern Alberta, Geology, 22, 683–686, https://doi.org/10.1130/0091-7613(1994)022<0683:ASLWLG>2.3.CO;2, 1994.